THESIS

EFFECT OF MIXED-MODE LOADING ON FATIGUE AND FRACTURE ASSESSMENT OF A STEEL TWIN BOX-GIRDER BRIDGE

Submitted by

Mazin M. Irfaee

Department of Civil and Environmental Engineering

In partial fulfillment of the requirements

For the Degree of Master of Science

Colorado State University

Fort Collins, Colorado

Spring 2019

Master's Committee:

Advisor: Hussam Mahmoud

Paul Heyliger
Rebecca Atadero
Lisa Stright

ABSTRACT

EFFECT OF MIXED-MODE LOADING ON FATIGUE AND FRACTURE ASSESSMENT OF A STEEL TWIN BOX-GIRDER BRIDGE

Steel twin box-girders are considered an attractive option for the construction of bridges due to their basic design, simple form, and ease of creation. Despite their advantages, they are considered fracture critical and as such there is an additional mandate for these bridges to inspected more in depth. This causes their inspection cost to be approximately two to five times greater than that of bridges with non-fracture critical members. The required additional inspection in the U.S. is mainly driven by rare historical events of bridge collapse for bridges that were not steel twin box girders. In addition, the mandated additional inspection does not reflect the inherent level of redundancy in most bridges. Therefore, it is important to quantify the potential for fracture and the level of redundancy in steel two-girder bridges in general, and twin box girders in particular, to minimize their inspection cost. Recognizing the inherently large scatter in fatigue performance, evaluating crack propagation and potential for fracture should, however, be performed in a probabilistic manner using detailed models that represent accurate behavior of the bridge. In this study, a detailed numerical finite element model of steel twin tub-girder bridge is developed and crack growth analysis, potential for fracture of its main tubs, and its overall redundancy is evaluated. The crack growth analysis is performed using multi-mode linear elastic fracture mechanics while accounting for uncertainties in the random variables associated with crack propagation and fracture. The results of the crack growth analysis are utilized to develop fragility functions that specify inspection intervals versus probability of failure where failure is

characterized by dynamic crack growth. The analysis conducted to quantify the potential for fracture show distinct possible failure modes that vary from brittle fracture to ductile fracture. The extreme loading case shows that the bridge overall is not at risk of collapse. It is important to note that this conclusion cannot be generalized for all tub girder bridges since the level of redundancy is expected to vary between bridges depending on many factors such as girders geometries, plate thickness, fabrication, among others. However, the presented approach and the corresponding results provide a systematic way by which fracture critical bridges can be evaluated.

TABLE OF CONTENTS

LIST OF FIGURES

CHAPTER 1

INTRODUCTION

1.1 General Background and Statement of the Problem

In the first half of the 20th century several bridge failures caused a nationwide concern over vulnerability of steel bridges. One famous example is the collapse of the Point Pleasant Bridge over the Ohio River in 1967. The collapse was one of the deadliest accidents in the history of bridge failures. Examinations of the failure have shown that brittle fracture of a single eye-bar, which was part of the supporting system of the main span, caused the whole structure to collapse (NTSB 1967). Fig. 1.1 shows a picture of the Point Pleasant Bridge after the collapse. Brittle fracture is a type of fracture in which accrues sudden and without any sign of plastic deformation or yielding. The reason for the complete failure was attributed to the lack of redundancy in the bridge. Because of the Point Pleasant Bridge collapse and other bridge failures, the American Association of State Highway and Transportation Officials, AASHTO, started to classify bridges more strictly so that bridges vulnerable to complete collapse can be identified. A new category for bridges with fracture critical members (FCMs) was introduced. Further result of the Point Pleasant Bridge failure was the establishment of the National Bridge Inspection Standards (NBIS) through Federal Highway Administration (FHWA), which came into effect in 1971. The NBIS document specified procedures and frequency for inspections, minimum qualifications for bridge inspectors, and new reporting and documentation requirements.

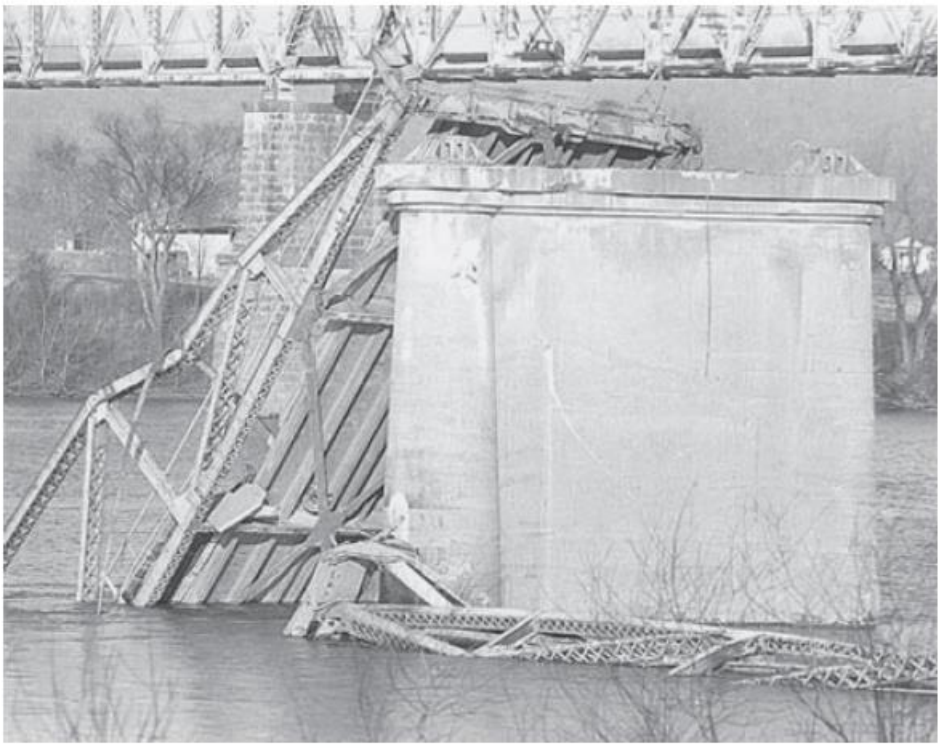

Fig. 1.1. The collapsed Point Pleasant Bridge (Connor et al. 2005)

Fracture critical members (FCMs) are defined in the 2017 AASHTO Specification (2017) as "*component in tension whose failure is expected to result in the collapse of the bridge or the inability of the bridge to perform its function*". Any bridge that has at least one fracture member is considered fracture critical bridge. Because of this definition, two-girder steel bridges are considered fracture critical and non-redundant. However, many previously conducted studies have shown various steel two-girder bridges to be highly redundant and not at risk of collapse when a full girder is fractured (Daniels 1989; Yakel et al. 2014; Idriss et al. 1995; Cha et al. 2014). A particular study on bridges with fracture critical details summarized examples of steel two-girder bridges that did not collapse due to the presence of a full depth fracture in one of its two girders (Connor et al. 2005). For example, in 1976 the US-52 bridge over the Mississippi River in St. Paul,

Minnesota (The Lafayette St. Bridge) had full depth fracture in one of its girders and it remained in service for 48 days before the fracture was discovered.

It is realized that the classification of bridges with respect to their redundancy is not simple. The problem, however, with classifying bridges as fracture critical is that such classification leads to hands-on inspection of fatigue cracks than necessary, which causes financial burden to bridge owners and tax payers. The rare occurrence of full collapse of fracture critical bridges, especially two-girder steel bridges, merits their classification as low probability events. However, they are indeed high-consequence events due to the expected monetary and life losses associated with their failures. Undoubtedly the tradeoff between financial burdens and safety (i.e. acceptable probability of failure) must be carefully considered. That is to say, some fracture critical bridges could be at high risk of fracturing and would indeed require more frequent periodic inspection. Therefore, proper quantification of the potential for loss of bridge functionality, due to bridge collapse, is critical for eliminating losses associated with such failures. This is particularly important for older bridges since various improvements to fatigue provisions were not introduced in the AASHTO Specification until mid-70's. Many of these bridges have already shown signs of cracking in many of their fatigue-prone details. Bridges designed and fabricated per modern fatigue provisions are less likely to experience fatigue cracks and subsequent fractures. Nevertheless, they are still required to adhere to the same inspection guidelines and are still required to be inspected periodically.

The importance of maintaining bridge functionality does not have to come at the cost of conducting periodic inspections that are not required. Therefore, it is important to devise new inspection intervals that are based on engineering analysis of crack growth and the potential for dynamic fracture and collapse rather than speculation of risk. It is important to note, however, that

although fatigue cracks are typically characterized by stable propagation rate, the scatter in fatigue performance is difficult to quantify and could be on the order of thousands or even millions of cycles. Therefore, the development of management programs for bridge structures should account for the inherent scatter in performance through probabilistic fatigue and fracture assessment.

In this study, fatigue and fracture assessment of a steel twin box-girder bridge is conducted. Specifically, probabilistic analysis is performed to assess the susceptibility of the girder to full depth fracture, defined by unstable crack growth. In the probabilistic analysis the crack growth parameters and the fracture toughness are treated as random variable. Furthermore, an extreme load case is conducted to evaluate redundancy of the bridge through quantifying the potential for full system collapse. While closed-sections, such as box girders, are characterized by their torsional stability, in the presence of large cracks extensive twisting of the girders could take place, resulting in additional introduced modes of cracking or failure. Therefore, in this study the fatigue and fracture assessment are performed using mixed-mode analysis. Mixed-mode refers to the case in which two or three modes of loadings (opening, sliding shear, and tearing) are present. In this study, fatigue crack growth is conducted using the Paris law for crack propagation while fracture assessment is conducted using the fracture assessment diagram to determine the acceptability of the crack size in relation to the potential for brittle fracture and net section collapse as well as to understand the mode of failure. The study conducted highlights the importance of utilizing mixed-mode analysis for fatigue and fracture assessment of bridges. The introduced framework also provides a systematic way for evaluating fracture critical bridges, which can be utilized by engineers for devising inspection intervals for bridges with FCMs.

1.2 Objectives

The overall goal of this study is to utilize comprehensive analysis methods to understand the behavior of a deteriorated twin steel girder bridge under modern AASHTO loadings requirements. this thesis sought to achieve the following:

- Observe the effects of second and third modes of fracture, generated due to changes to crack boundaries, on fatigue crack life.
- Calculate equivalent mode of fracture (mixed mode) that combines the three fracture modes to evaluate its effect on fatigue crack life.
- Investigate the relationship between crack length and stress intensity factor for mixed mode loading.
- Use Paris law model to simulate fatigue crack growth under mixed mode and compare it with first mode to understand the effect of mixed mode on fatigue crack propagation life.
- Utilize the fracture assessment diagrams (FAD) to estimate the failure type of the existing crack and evaluate the fracture locus.
- Use a probabilistic analysis as a tool to evaluate the effects of statistical variations in the Paris law constants and material toughness on crack growth.
- Predict the potential of bridge collapse if one of its girders fully fractured.
- Evaluate the effects of cross frames on the redundancy of two-girder steel bridges, through their contribution in generating alternative load paths.

1.3 Scope of Research

To achieve the abovementioned goals, the work conducted for this study was limited in scope to the following:

- Conduct comprehensive literature review focusing on fundamentals of fracture mechanics, tools to evaluate fatigue crack life, and behavior of twin-girder steel bridges.
- Develop 3-D twin girders steel bridge finite element model (FEM) to simulate crack propagation using AASHTO, 2017 loads requirements.
- Use the same 3-D model to simulate the effects of transverse bracings and diaphragms on fatigue crack life and bridge redundancy.
- Utilize the output of the FEM to conduct probabilistic fatigue and fracture assessment.
- Interpret the FEM results to evaluate fatigue crack life and failure modes.
- Interpret the results to devise inspection intervals using the results of the probabilistic analysis.
- Assess pros and cons of using cross frames on fatigue crack life and bridge redundancy.

1.4 Organization of Thesis

This thesis includes five different chapters. Chapter 1 introduces the problem statement, motivations, and objective of this research. Chapter 2 discusses background and literature review in reference to assessment of behavior of twin-girder steel bridges with focus on fatigue crack propagation and fracture. Chapter 3 concentrates on the methodology used to evaluate fatigue crack growth and fracture as well as details of the developed finite element model. Chapter 4 presents interpretation of the FEM results and the use of the results in probabilistic fatigue and

fracture assessment. Chapter 5 summarizes the findings from the current study and includes suggestions for future research.

CHAPTER 2

BACKGROUND AND LITERATURE REVIEW

2.1 Introduction

The focus of the literature review on fatigue and fracture of metal alloys with application to two-girder steel bridges. As such, in this background section basic knowledge of design specifications, evaluation methods for fatigue crack initiation and propagation, and evaluation methods for failure modes are provided.

2.2 Fundamentals of Fatigue and Fracture Mechanics

The fundamentals of fracture mechanics field were relatively matured by the end of the 20th century and current research tends to provide only incremental progress in this field. Therefore, many recent studies have been geared more towards applications rather than theoretical development. In steel bridges, the primary field of application pertained more to fatigue cracking since fatigue cracks constitute the majority of problems in the bridges with very limited cases of fracture. Fatigue cracking is the processes in which initiation and propagation of a crack is manifested due to repeating action of cyclic loading (Fisher et al. 1998). The crack initiation and propagation stages are primarily influenced by the cyclic loads, stress range introduced in the materials from the loads, and the directions of the loads. The directionality of theses loads is the primary factor influencing the fracture mode in the material. Previous fracture mechanics studies had led to complete understanding of the effects of the three principals loading modes on crack development and directionality.

Fracture mechanics can also be defined as the field concerned with investigation of initiation and propagation of cracks in materials. Modern perspective on mechanics of materials realized the importance of fracture mechanic as a tool to improve material performance under applied loads. Specifically, the physics of stress and strain fields in materials in elasticity and plasticity theories are typically used to investigate the potential for failure.

2.3 Fracture Modes

There are three fracture modes a crack can experience, and each mode represent a unique case of loading depending on type and direction of the load. Mode I, also known as opening mode, occurs when normal stress acts perpendicular to the crack plane, causing the crack to open. Mode II, or sliding mode, is present when shear stresses act parallel to the crack plane causing the crack faces to slide along each other. Mode III, or tearing mode, occurs when out-of-plane shear stresses act parallel to the crack faces and perpendicular to the cracked member or the element, causing the crack tip to tear. Fig. 2.1 illustrates the fracture modes and loading direction for each mode. A crack can experience one predominate mode or a combination of modes, causing the crack to propagate until it reaches the fracture limit state. Although mode I represents most of the cases, there are conditions in which combined modes are present. These include for example out-of-plane distortion in which cross frames or floor beams are deforming in way that causes distortion in the main girder web, resulting in mode I and III being the main contributors to cracking.

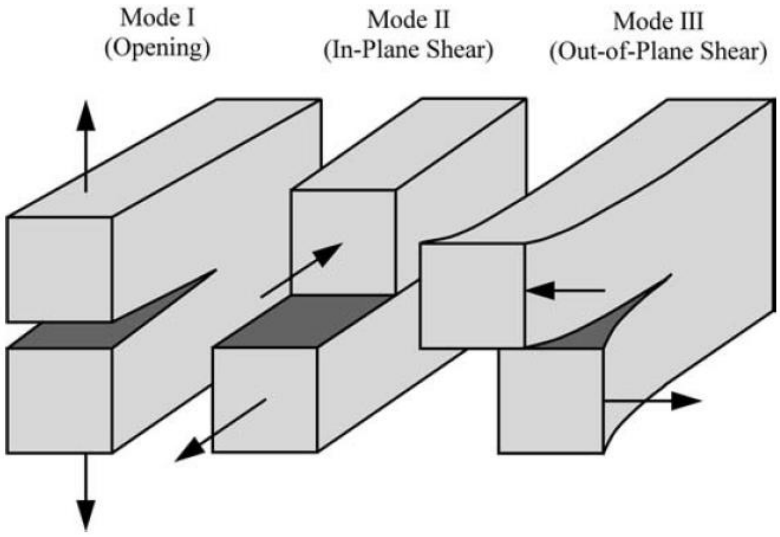

Fig. 2.1. The three fracture modes (Anderson,2005)

2.4 **Linear Elastic Fracture Mechanics**

The linear elastic fracture mechanics (LEFM) concept was first developed in 1921 by Griffith and it was only used for materials that comply to Hook's law where the behavior is linear elastic. Since 1921, LEFM concept have been used in various fatigue and fracture applications. Early use of LEFM pertained to defining energy and stress intensity as a way of determining the potential for crack extension. At the atomic level, fracture occurs when stress and work cause the bonds between the atoms to break. The atomic bond represents the attracting forces between these atoms, which determine material strength. The equilibrium between the atoms mainly depends on the spacing between atoms where if a tension force is applied and it is larger than the potential energy, the distance between the atoms will increase causing atom separation. Fig. 2.2 describes the relationships between the energy, forces, and the separation distance between the atoms. The

relationship between the atoms can be defined using the cohesive strength theory (σ_o) as the following (Anderson, 2005):

$$\sigma_o = \frac{E\lambda}{\pi x_o} \tag{2.1}$$

Where σ_o is the cohesive stress, E is the elasticity modulus, x_o is the equilibrium spacing, λ is the spacing between two atoms. If the spacing between two atoms is assumed to equal the equilibrium spacing, then the cohesive stress approximately equal E/π (~10,000 ksi). This is an unrealistically large number that cannot hold true since experimental tests have shown the fracture stress for metal alloy (e.g. steel) to be much smaller than this value. This unrealistically high value is due to the fact that the calculated cohesive stress does not account for the presence of flaws in the material. It is important to note that equilibrium spacing is the spacing at which the potential energy is at minimum. As a result, to achieve complete separation between two atoms a tension force that is larger than cohesive force is required. The cohesive stress can also be estimated using the surface energy per unit area (γ_s). Since material fracture comprises of two surfaces, γ_s equal to half the fracture energy and can be calculated as follows:

$$\gamma_s = \frac{1}{2}\int_0^{\lambda} \sigma_o \sin\left(\frac{\pi x}{\lambda}\right) dx = \sigma_o \frac{\lambda}{\pi} \tag{2.2}$$

Finally, the cohesive stress as function of γ_s can be estimated as the following:

$$\sigma_o = \sqrt{\frac{E\gamma_s}{x_o}} \tag{2.3}$$

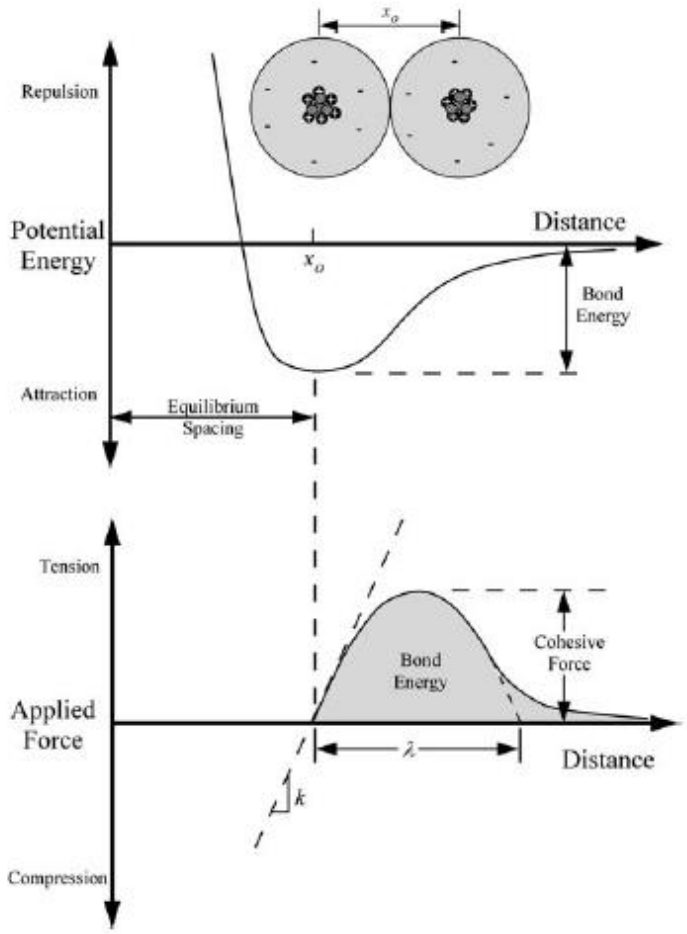

Fig. 2.2. Potential energy and force as a function of atomic separation (Anderson, 2005)

2.4.1 Stress Concentration

In (1913) Inglis developed a fracture model for a flat plate with center elliptical crack to evaluate materials strength in the presence of a flaw. This model was built on the notion that at the atomic level fracture will not occur unless the applied load was larger than the cohesive strength (Anderson, 2005). In addition, the presence of a flaw makes the material overall strength lower than the local stresses at the flaw (Anderson, 2005). Fig. 2.3 shows the model proposes by Inglis

where σ is the applied stress, $2a$ is the crack length, $2b$ the crack width, and ρ is the crack tip curvature.

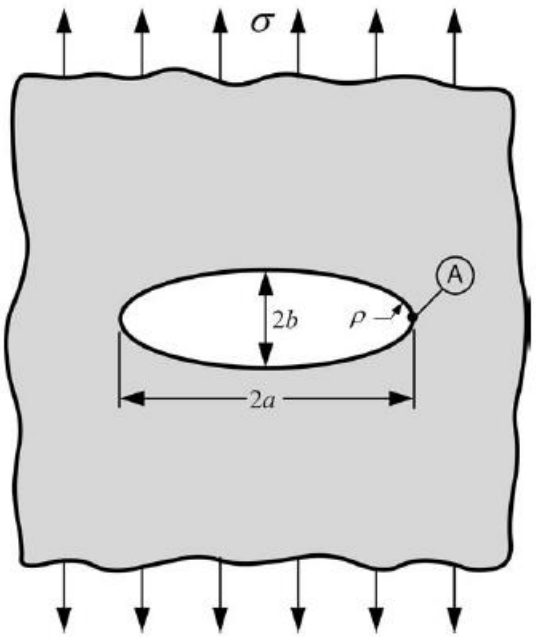

Fig. 2.3. Assumptions of Griffith model (Anderson, 2005)

The results of this model is a closed-form solution to estimate the stress concentration at Point A, which represents the crack tip:

$$\sigma_A = \sigma\left(1 + \frac{2a}{b}\right) \tag{2.4}$$

Another form for this equation in terms of the crack tip curvature, ρ, and when a is increasing relative to b so that the crack shape is in the form of an ellipse:

$$\sigma_A = \sigma\left(1 + 2\sqrt{\frac{a}{\rho}}\right) \tag{2.5}$$

Where ρ is defined as the following:

$$\rho = \frac{b^2}{a} \tag{2.6}$$

Inglis noted that the most common and critical case for a crack is when the tip is sharp. Therefore, based on this assumption the stress at point A, when $a>>b$, can be written as:

$$\sigma_A = 2\sigma\sqrt{\frac{a}{\rho}} \tag{2.7}$$

Using the same stress field at point *A*, the local stress field at the crack tip at the atomic level, where ρ equals to the equilibrium spacing (x_o), can be determined as:

$$\sigma_A = 2\sigma\sqrt{\frac{a}{x_o}} \tag{2.8}$$

Furthermore, in assuming that the local stress at the crack tip equal to the cohesive stress, the normal stress at the onset of failure can be estimated as per equation (2.9):

$$\sigma_f = \left(\frac{E\gamma_s}{4a}\right)^{\frac{1}{2}} \tag{2.9}$$

2.4.2 Energy Balance

In 1920 Griffith developed another fracture model based on energy balance using Inglis model (1913) as a reference. This energy approach was based on the premise that reduction in material total energy occurs when the material goes from a nonequilibrium state to an equilibrium state, which is the first law of thermodynamics. One of the reasons for developing this model was due to concerns raised when using the 1913 model by Inglis in which the stress concentration tends to infinity as a result of setting ρ = 0 for very sharp crack. The Griffith model was based on the concept of crack formation and growth under condition of total energy balance. In setting his model, Griffith assumed that the crack length (*2a*) is very large compared to plate thickness (*b*) *2a*>>*b*, and that the plate is subjected to uniform and constant stress (σ). The Griffith model (1921) was built using the concept of incremental increase in the crack area (*dA*) under energy balance condition where the crack size increased when the potential energy remained in the plate overcame

the surface energy. This relationship between the crack incremental area and the energy can be defined as following:

$$\frac{dE}{dA} = \frac{d\Pi}{dA} + \frac{dW_S}{dA} = 0 \tag{2.10}$$

Or

$$-\frac{d\Pi}{dA} = \frac{dW_S}{dA} \tag{2.11}$$

Where E is total energy, Π is potential energy provided by the internal strain energy and external forces, and W_S is work needed to generate a new surface. The results of compiling both models Griffith and Inglis is as follows:

$$\Pi = \Pi_o - \frac{\pi\sigma^2 a^2 B}{E} \tag{2.12}$$

Where Π_o is the potential energy for uncracked plate and B is the plate thickness. As previously noted, to generate a crack two surfaces are needed. The work needed to create the crack surfaces can be expressed as follows:

$$W_S = 4aB\gamma_s \tag{2.13}$$

Where γ_s is the materials surface energy. Then

$$-\frac{d\Pi}{dA} = \frac{\pi\sigma^2 a}{E} \tag{2.14}$$

and

$$\frac{dW_S}{dA} = 2\gamma_s \tag{2.15}$$

Combining equations 2.14 and 2.15 to solve for the failure stress results:

$$\sigma_f = \left(\frac{2E\gamma_s}{\pi a}\right)^{\frac{1}{2}} \tag{2.16}$$

Furthremore, the Griffith approach not only it can be used for calculating the failure stress for a sharp crack but also for other crack shapes such as a penny shape crack and embedded penny-shaped crack expressed as follows:

$$\sigma_f = \left(\frac{\pi E \gamma_s}{2(1-\upsilon^2)a}\right)^{\frac{1}{2}} \quad (2.17)$$

Where a is the crack radius and υ is Poisson ratio.

2.4.3 The Energy Release Rate

In 1956, a similar model to Griffith's model was proposed by Irwin (1956) to solve fracture problems. The new approach was called Energy release rate G which estimates the energy field at growing crack increment, and it can be defined as follows:

$$G = -\frac{d\Pi}{dA} \quad (2.18)$$

The main premise of this approach is to assess the potential energy change rate with crack area. Comparing the pervious approach with the energy release rate approach, G becomes:

$$G = \frac{\pi\sigma^2 a}{E} \quad (2.19)$$

And the critical value for energy release rate G_c becomes:

$$G_c = \frac{dW_s}{dA} = 2W_f \quad (2.20)$$

Where G_c presents the fracture toughness for the material. For elastic materials the potential energy Π is:

$$\Pi = U - F \quad (2.21)$$

Where U is internal strain energy for the materials and F is the external force. Irwin approach for the energy release rate can be applied for the case of load control and displacement control. Fig. 2.4 (a) illustrates Irwin model for the load control case in which a cracked plate is loaded with fixed load P. Fig. 2.4 (b) explains the relationship between the load and the displacement. To

estimate the potential energy field around the crack for this case can be realized using the following steps:

$$F = P\Delta \tag{2.22}$$

Where P is the load and Δ is the displacement, then:

$$U = \int_0^{\Delta} P d\Delta = \frac{P\Delta}{2} \tag{2.23}$$

Therefore:

$$\Pi = -U \tag{2.24}$$

And finally,

$$G = \frac{1}{B}\left(\frac{dU}{da}\right)_P = \frac{P}{2B}\left(\frac{d\Delta}{da}\right)_P \tag{2.25}$$

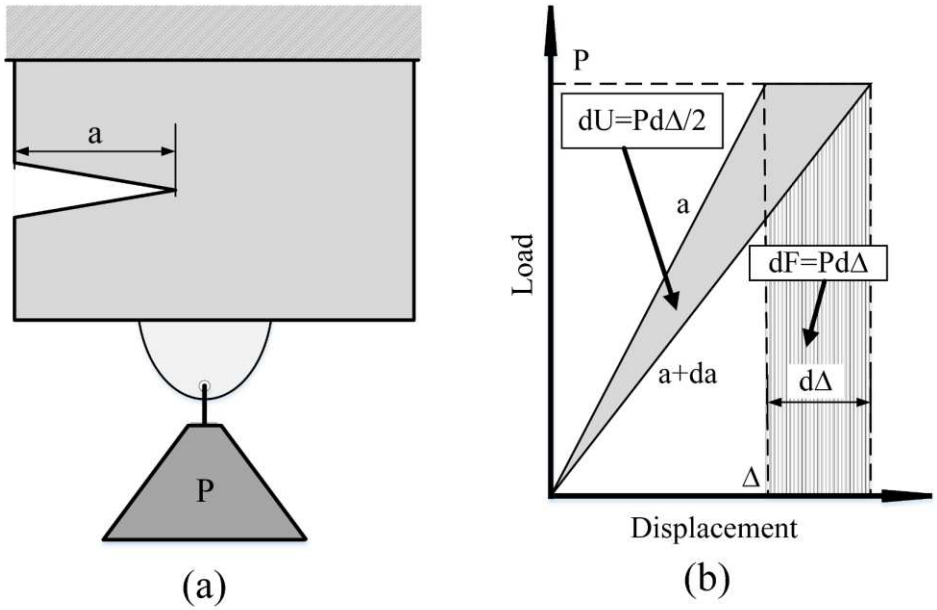

Fig. 2.4. (a) Irwin model Load controlled, (b) the relationship between load and displacement (Anderson, 2005)

For the second case which is displacement control, the displacement is assumed fixed and the load is changing. Fig. 2.5 (a) shows schematic of Irwin's model for this case. Fig. 2.5 (b) shows the

corresponding relationship between the load and the displacement. Since the displacement is fixed, then F=0 and Π=U. As a result, the expression for the energy release rate is as follows:

$$G = -\frac{1}{B}\left(\frac{dU}{da}\right)_{\Delta} = -\frac{\Delta}{2B}\left(\frac{dP}{da}\right)_{\Delta} \tag{2.26}$$

Based on the above discussion, it follows that the energy release rate under load control is negative of that under displacement control.

$$\left(\frac{dU}{da}\right)_{P} = -\left(\frac{dU}{da}\right)_{\Delta} \tag{2.27}$$

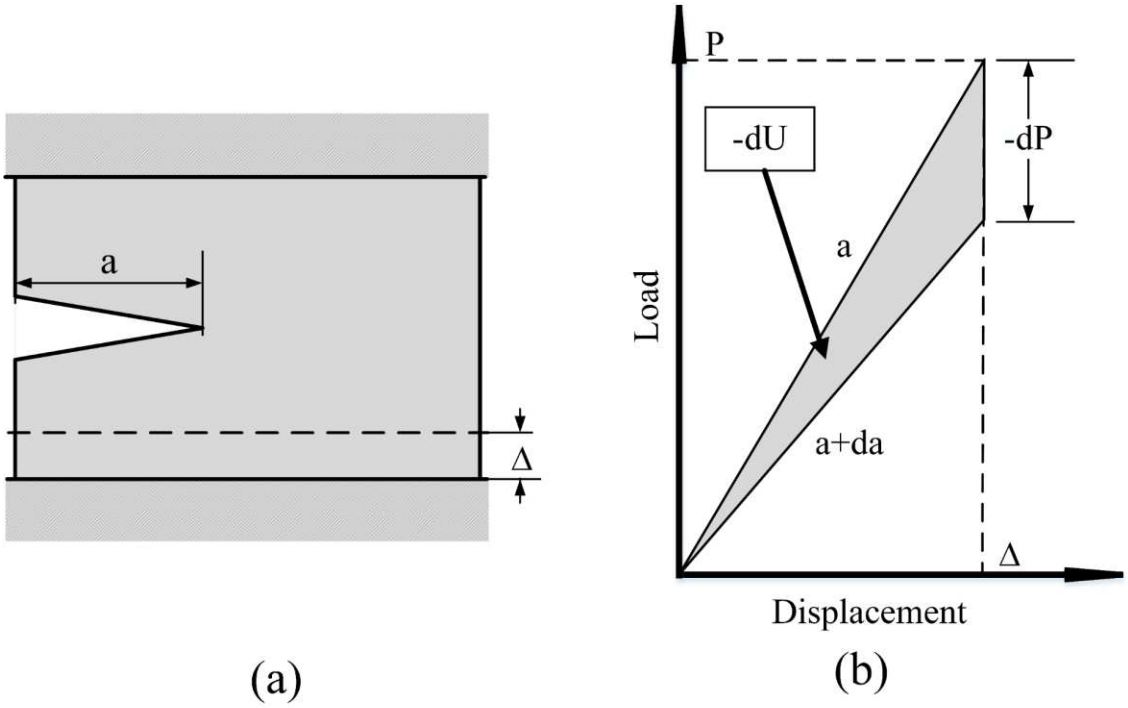

Fig. 2.5. (a) Irwin model Displacement controlled, (b) the relationship between load and displacement (Anderson, 2005)

Equation (2.27) explains the relationship between the load and that shown in Fig. 4 (b) and 5 (b) where in the load-control case, the incremental crack growth *da* occurs because of the net increase in strain energy as a result of increasing the load *P*:

$$(dU)_P = Pd\Delta - \frac{Pd\Delta}{2} = \frac{Pd\Delta}{2} \tag{2.28}$$

For the second case, where the displacement is fixed and dF=0, the strain energy decreases:

$$(dU)_{\Delta} = \frac{\Delta dP}{2} \tag{2.29}$$

Where dP has a negative sign as shown in Fig. 2.4 (b) and 2.5 (b). The absolute energy values for both cases differ by $dPd\Delta/2$, which is very small and should be ignored. As a result for an increment of crack propagation da at a given load P and displacement Δ.

:

$$(dU)_P = -(dU)_{\Delta} \tag{2.30}$$

Finally, when consideration the plate compliance, C, which is the inverse of the stiffness, the solution becomes:

$$G = \frac{P^2}{2B}\frac{dC}{da} \tag{2.31}$$

2.4.4 Stress Intensity Factor, SIF (K)

The stress intensity factor approach was devolved by Irwin, 1957. Stress intensity factor is a value that describes and estimates the stress field near the crack tip that result of the loads and residual stresses based on linear elastic behavior. However, this concept still applies for materials that show small scale of yielding at crack tip. Stress intensity factor is used in many applications to evaluate the crack propagation rate in term of crack length such as Paris low, and the failure due to presence of a crack using the material toughness and failure stress as limit states such as failure assessment diagrams based on. The units for stress intensity factor are MPa√m or ksi√in, which are stress unit in square root of length unit. Stress intensity factor is expressed as the following:

$$\sigma_{ij}(r,\theta) = \frac{K}{\sqrt{2\pi r}} f_{ij}(\theta) \tag{2.32}$$

Where K is stress intensity factor, σ_{ij} is stress, (r, θ) are polar coordinates and Fig. 2.6 demonstrate these coordinates, and f_{ij} are dimensionless functions that depend on the loading condition, element geometry, and structural component.

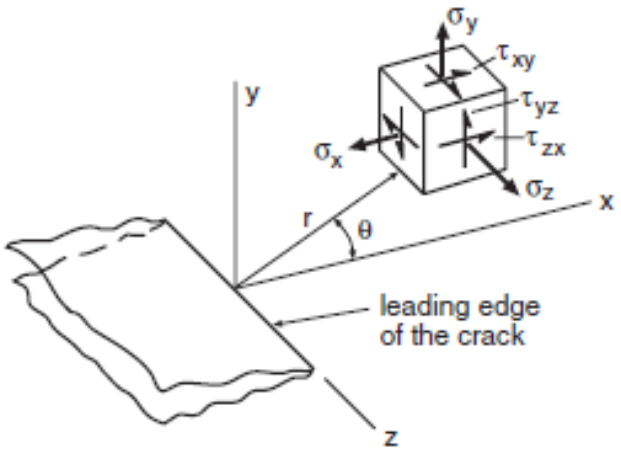

Fig. 2.6. The polar coordinates for stress intensity factor mathematical form (Dowling, 2013)

Stress intensity factor symbol, K usually has subscript from one to three that represent the stress intensity factor mode. These three modes depend on the loads condition and direction and they are defined as the following:

$$K_I = \lim_{r \to 0} \sqrt{2\pi r}\, \sigma_{yy}(r, 0) \tag{2.33}$$

$$K_{II} = \lim_{r \to 0} \sqrt{2\pi r}\, \sigma_{yx}(r, 0) \tag{2.34}$$

$$K_{III} = \lim_{r \to 0} \sqrt{2\pi r}\, \sigma_{yz}(r, 0) \tag{2.35}$$

Fig. 2.7 shows three modes and illustrates how the load direction represents each mode.

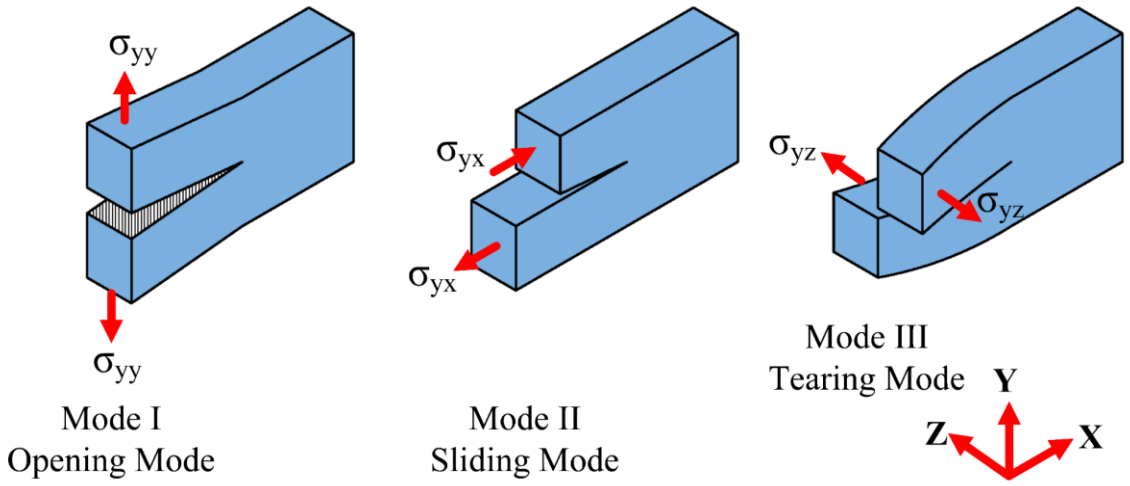

Fig. 2.7. The different modes for Stress intensity factor, K and the load direction for each mode (modified after Anderson,2005)

In addition, there is simpler form to calculate the stress intensity factor and it can be defined as the following:

$$K = Y\sigma\sqrt{\pi a} \tag{2.36}$$

Where Y are dimensionless functions and a is half the crack length for a center crack. Furthermore, although the stress intensity factor built on linear elastic fracture mechanics principle it still valid to use if there are small scale of plasticity around the crack tip. The small scale plasticity region around the crack tip called plastic zone, and this plastic zone can be corrected for so that LEFM can still be used. Irwin (1961) proposed that this correction can be realized by using an effective crack length a_{eff} which includes the plastic zone as part of the crack length in order to estimate an effective stress intensity factor K_{eff}. The effective crack length a_{eff} is expressed as follows:

$$a_{eff} = a + r_y \tag{2.37}$$

Where r_y is the radius of the plastic zone and can be estimated as follows:

$$r_y = \frac{1}{\pi}\left(\frac{K}{\sigma_{YS}}\right)^2 \tag{2.38}$$

Where σ_{YS} is yield stress. Then, the effective stress intensity factor becomes:

$$K_{eff} = Y\sigma\sqrt{\pi a_{eff}} \tag{2.39}$$

2.5 Fatigue Crack life

Fatigue crack life starts when the stress or the loads applied to an element in a repeating manner reaches the stress range threshold that causes material atoms to separate. After the stress threshold is reached fatigue crack life can be classified into three phases which are initiation, propagation, and fracture or failure. The crack initiation phase is the time period that a crack takes from the moment stress reached the limit state that results atoms separation until the crack shows up on the element surface. The propagation phase is the time the crack takes from the moment it appears on the surface (assuming it was an embedded crack) until it propagates across the width of the entire element. The fracture or failure phase is simply failure when the crack length becomes too large for the material to tolerate.

2.5.1 Fatigue Crack Initiation

Fatigue crack initiation is the phase where the stress range of the repeated cyclic load reaches the limit that can cause the material to start separating at the atom level. The crack initiation life is the time or number of cycles it takes for a crack to appear on the element surface. There are many methods used to evaluate this phase of fatigue crack life, one of the most commonly used method is the S-N curves. S-N curves are simply curves that represent the relationship between the stress range and the number of cycles for certain material to define failure or crack initiation. S-N Curve

mainly consists of four elements which are Y-axis (stress range), X-axis (number of cycles), assessment line, constant amplitude fatigue limit (CAFL). The stress range axis represents the nominal stress applied to the detail. The number of cycles axis represents the cycle count in which crack initiation is expected based on the applied stress range. The assessment line is used to estimate the fatigue initiation life (i.e. relationship between stress range and number of cycles). The CAFL line present the stress range below which an infinite life is expected. Fatigue details are categorized based on their fatigue life and as such they are grouped into different categories (from A to E') that are represented by different S-N curves. Fig. 2.8 illustrates how an S-N curve can be used to define the onset of crack initiation and Fig. 2.9 shows the S-N curves for all fatigue categories according to AASHTO (2017).

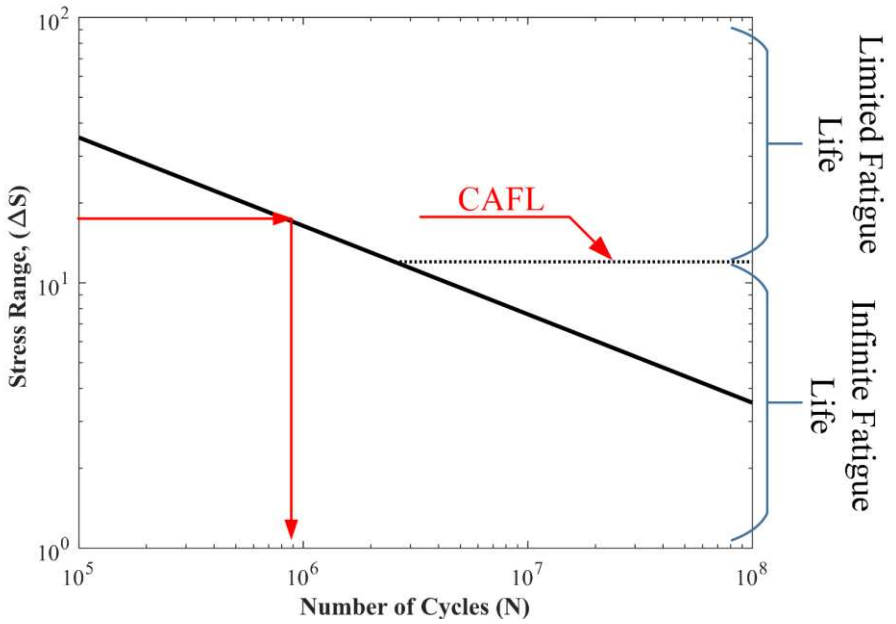

Fig. 2.8. S-N Curve Definition

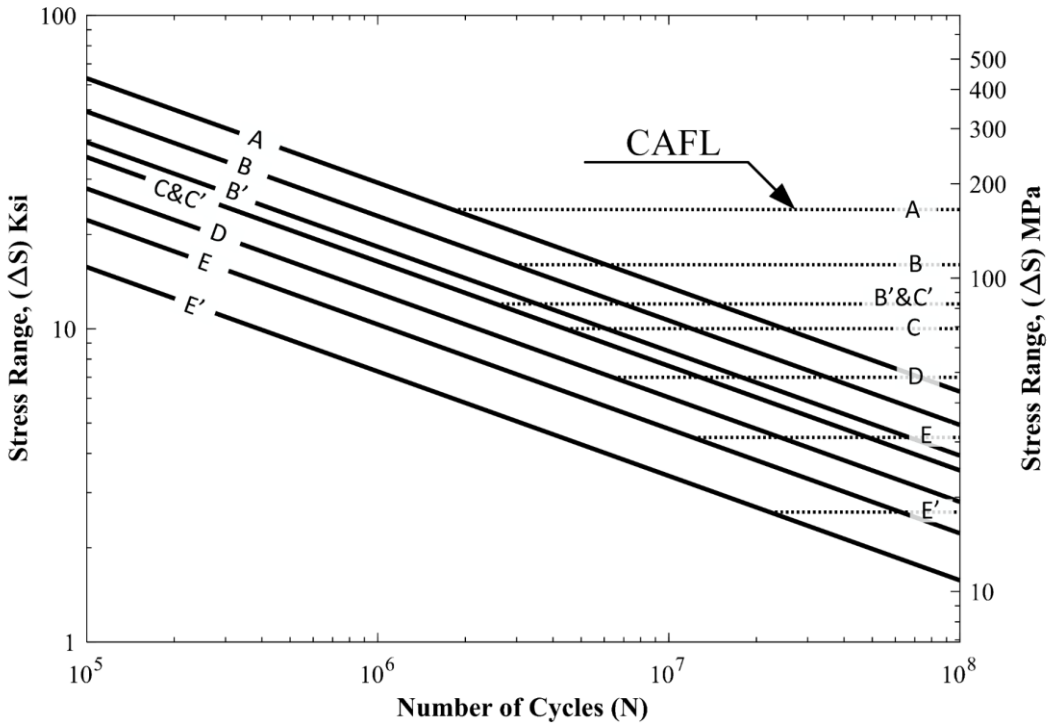

Fig. 2.9. AASHTO (2012) S-N Curve for all fatigue details

2.5.2 Fatigue Crack Propagation

The fatigue crack propagation stage represents the second phase of the crack life which is the time from when the crack becomes a through thickness crack until its complete propagation across the plate width. The propagation rate of a crack could be unstable or stable, depending on the relationship between the crack size, the stress intensity around the crack, among others. This relationship has been defined by many models such as (Paris and Edorgan (1963), Walker (1970), Forman (1972), McEvily (1974), Zheng (1983), Wang et al. (1994), Beden et al. (2009)). The most used model is that by Paris and Edorgan (1963) who proposed a relationship between the range in stress intensity factor, ΔK, with fatigue crack growth in the form of incremental number of cycles, dN for each crack length increment, da. Known as the Paris law, this relationship is defined as follows:

$$\frac{da}{dN} = C(\Delta K)^m \tag{2.40}$$

Where *da* is the crack length increment, *dN* is the number of cycles that correspond to da, *C* and *m* are materials coefficients that depend on the materials properties and geometry, and ΔK is the range of stress intensity factor. The range of stress intensity factor, ΔK is calculated as follows:

$$\Delta K = K_{max} - K_{min} \tag{2.41}$$

The Paris law divides the fatigue crack propagation life into three regions where each region describes a propagation state. The three propagation states are no growth, stable propagation, and unstable propagation to failure. The divisions of these regions were built based on ΔK values and Fig. 2.10 shows these three regions and illustrates how ΔK value controls the growth. Where K_{th} is stress intensity factor threshold, and K_{IC} is the material toughness. The crack will have infinite fatigue life and no growth will occur if ΔK is smaller than K_{th}, but if K_{max} is larger than K_{IC} the crack will grow in an unstable matter, causing the element to fail. It is worth noting that the Paris law model is based on linear elastic mechanics for mode I. However, extension of the Paris law for other modes have been the subject of some studies as will be explained in details in the next chapter.

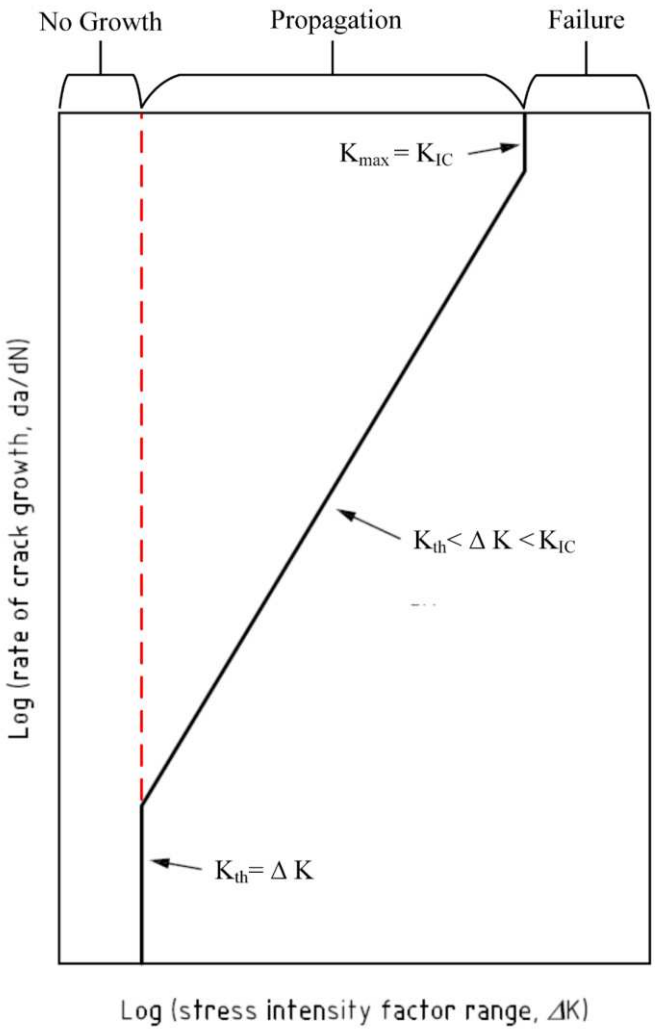

Fig. 2.10. Paris law crack growth relationship (BS 7910, 2015)

2.6 **Type of Fracture**

The nature of fracture is classified into three different types including brittle failure, ductile failure, and transition fracture, which is a mixed mode of failure that combines brittle and ductile fractures. Brittle failure is most dangerous of the three because it does not provide any warring sign in the form of plastic deformation. Brittle fracture occurs when the stress intensity factor around crack tip reaches the material toughness, but the nominal stress has not reached the yield. Brittle fracture

causes the crack to propagate unstably under dynamic growth resulting in element separation. Ductile failure on other hand occurs when the nominal stress, in proximity to the crack, reaches the yield stress, but the stress intensity at the crack has not reached the materials toughness. For this kind of failure, the element fails due to plastic collapse where obvious necking occurs on the cross section. The transition failure mode, which is a mixed mode between brittle and ductile modes, occurs when the element fails as a result of the stress intensity factor being near the material toughness in the presence of large plastic deformation. In this mode, the failure cross section takes different shapes along the section where some places have smooth surface, indicative of brittle fracture, followed by yielded surfaces. Many models have been introduced for each mode. The Failure Assessment Diagrams (FADs) has been a popular model to use since it combines all three modes in one diagram. FADs were introduced by BS7910 (2015) which it consists of three parts which are fracture axis (K_r), collapse axis (L_r), and the assessment line. The fracture axis is the Y axis and it represents the ratio between the SIF and the material toughness. The collapse axis is the X axis and it represents the ratio between the yield stress and nominal stress on the remaining cross section that has not cracked. The assessment line represents the relationship between the fracture axis and the collapse axis to determine the failure mode brittle, ductile, or mixed. The assessment line is also used to determine if the crack is acceptable or not where if a point that represent both axes landed in the region bounded by the assessment line then the flaw is acceptable and if it landed outside of that region then the crack is not acceptable, and failure has been reached. Fig. 2.11 shows a depiction of the FAD. More information and details on FADs are included in the next chapter.

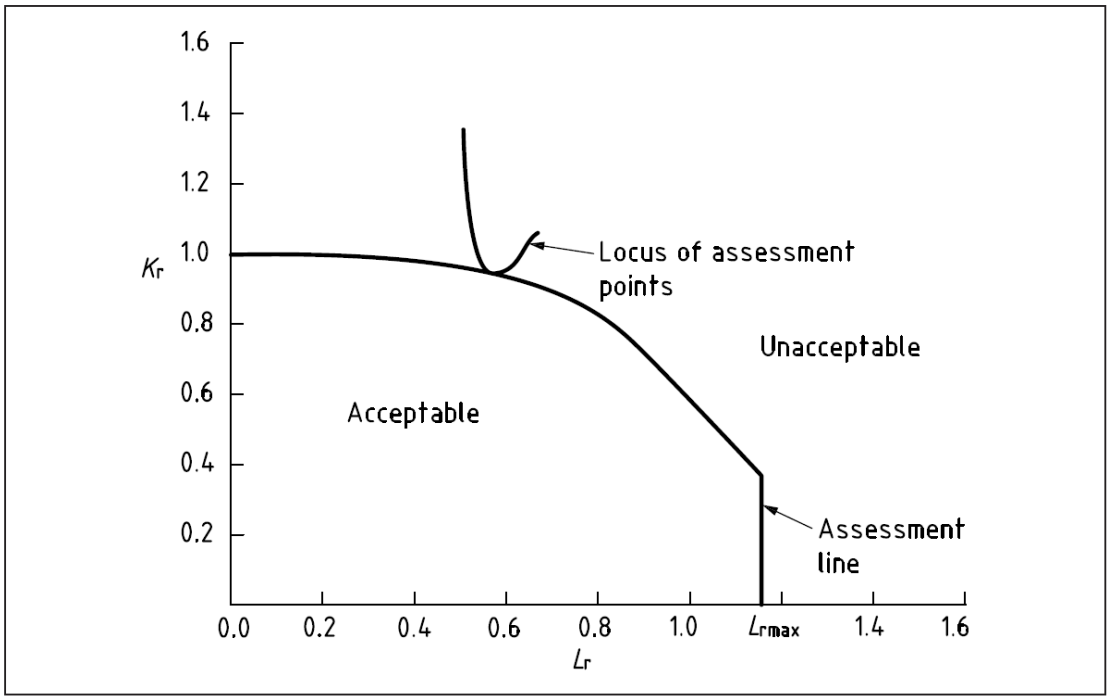

Fig. 2.11. An example for FAD illustrates how it functions and look like (BS79010, 2015)

2.7 Fracture Critical Bridges

2.7.1 Introduction

Fracture critical members are defined by the American Association of State Highways and Transportation Officials as "component in tension whose failure is expected to result in the collapse of the bridge or the inability of the bridge to perform its function" (AASHTO, 2017). In addition, any bridge that has at least one fracture critical member is considered a fracture critical bridge. As results of this definition two girders steel bridges are classified as critical and non-redundant by AASHTO (2017). However, many studies concluded that two girders steel bridges do not fit this definition (Daniels 1989, Yakel et al. 2014, Idriss et al. 1995, Cha et al. 2014). These

studies linked the complete collapse of FCBs with system redundancy to prove that two girder bridges have the ability to transfer the loads through other mechanisms (e.g. secondary members or deck catenary action) to prevent collapse.

Although, using fracture critical bridges are not prohibited, special requirements are enforced for the design, fabrication and hands-on inspection of these bridges. These requirements, implying an added cost, are the main the reason bridges owners prefer to avoid using these kinds of bridges. However, that only solves the problem partially because there is a reasonable number of FCBs in the United States' bridge inventory. Specifically, FCBs represent around 11% of bridges in U.S., and 80% of those bridges are two girders steel bridges. Some of these bridges were constructed before 1975, which is prior to the fatigue provisions being fully matured. Bridges constructed using modern fatigue provisions are at smaller risk of devolving fatigue cracks. However, these bridges are still treated the same way in terms of inspection requirements.

2.7.2 Studies on Two-girder steel bridges

Many studies that have been conducted on two girder steel bridge concluded that some of these bridges are highly redundant. A comprehensive study by Connor et al. (2005), titled "Inspection and Management of Bridges with Fracture Critical Details", summarized many cases of two-girder steel bridges that did not collapse when one of the girders had full depth fracture. In addition, this study concluded that under some circumstances two-girder steel bridges do not meet the definition of fracture critical bridges (FCBs) because of their inherent level of redundancy once a girder fractures. For example, in 1976 the US-52 bridge over the Mississippi River in St. Paul, Minnesota (The Lafayette St. Bridge) had full depth fracture in one of its girders and it is remained functioning for 48 days before the fracture was discovered. Fig. 2.12 shows the fully fractured girder.

Fig. 2.12. The Lafayette St. Bridge fully fractured girder (Connor et al. 2005)

Another study was conducted by NCHRP (Daniels, 1989) named "Recommended Guideline for Redundancy Design and Rating of Two-girder steel bridges," confirmed that two-girder steel bridges remain serviceable and fully functioning when one girder fractures. This study illustrated that increase in cross connection between the girders, such as lateral bracings, provides alternative loads paths that redistributes the loads and keeps the bridge serviceable after full fracture of one of the girders.

Another study that was conducted by Yakel et al. (2014) included experimental testing of full scale two-girder steel bridges to evaluate the level of redundancy in the bridges in case of full fracture of one of the girders. This study concluded that redundancy in two-girder steel bridges should classify them as "non-fracture critical". The study further highlighted the importance of revisiting the two-years requirement of hands-on inspection for two girder bridges.

Another study that conducted by Idriss et al. (1995) for 1-40 bridges over the Rio Grande in Albuquerque, New Mexico concluded that the bridge was stable when a mid-depth fracture was introduced in one of the girders in three-span unit. The study illustrated that the maximum vertical deformation of the bridge was 30.1625 mm under dead and live load without any yielding. Additionally, this study proved that the load redistributed in the three-dimensional structure by both primary and secondary members, through the deck, stringers, floor beams, and bottom lateral bracing.

Another study was conducted by Cha et al. (2014) to investigate after fracture redundancy level under several cases of loading for trussed system of two-girder steel bridges. This study considered The U.S.-421 Milton Madison Bridge. Using experimental and numerical analysis, the study showed that losing the primary member such as the cord will not cause complete collapse.

All these previous studies have proven that two-girder steel bridges have high level of redundancy that allow loads to transfer through other members and actions to prevent the bridge from collapsing. This points to the conclusion that hands-on inspection of two girder bridges every two years is very conservative and that cost savings could be realized if proper inspection intervals are devised based on true risk.

2.7.3 Studies on Twin Box-Girder Steel Bridges

Twin box–girder steel bridges are very attractive to be used because they have high level of redundancy and special torsion resistance because of the unique structure of their cross-section. Twin box–girder steel bridges are used along highways everywhere in the United States and have shown excellent performance in supporting their intended function (Pham et al. 2016). Despite their advantages twin box–girder steel bridges, similar to two-girder steel bridges, have been classified as fracture critical bridges because they contain fracture critical members. Various

studies have been conducted to prove that twin box–girder steel bridges can support loads with fully fractured FCM. Few of these studies are summarized below:

In 2016, a study was conducted by Pham et al. (2016) sponsored by Florida DOT was aiming to remove twin box–girder steel bridges from the list of fracture critical bridges. In their study, small scale and full-scale sections of twin box–girder steel bridge experiments and finite element models were used. The study showed that twin box–girder steel bridges are highly redundant and can survive fully fractured girder. The study showed however that different loading configurations and different bridge structure, formed by secondary elements, can alter (increase or decrease) the level of redundancy.

In 2010, a study was conducted by Barnard et al. (2010) to test the level of redundancy in twin box–girder steel bridges where full-scale model and numerical FEM model were utilized. To estimate the level of redundancy this study assumed a worst-case scenario by placing an HS-20 standard design truck as live load above the location where one of the girders was fully fractured. In addition, this study considered two different span systems, one continues and the other was simply supported, to evaluate the behavior of different span systems. The results indicated that continues-span system of twin box–girder steel bridge is very redundant where it can carry a full live load without risk of collapse or major damage when one of the girders is fully fractured. The study stated that continues-span system developed cantilever action mechanism where all the loads transferred to other spans. However, the simply supported system showed some weaknesses where some of the shear studs slipped near to location where the girder was fractured.

In 2009, a study was conducted by Neuman, B (2009). The study main objective was to quantify the level of redundancy in twin box–girder steel bridges. Full-scale specimens of twin box–girder steel bridges were utilized to be field tested using several loading scenarios. The conclusion made

based on these field tests was that twin box–girder steel bridges are not at risk of collapse with a fully fractured girder. Even with one of the tests being designed to reach the collapse, only partial collapse occurred at the location where the girder fully fractured under four times the design truck load. It was noted in the study that even with different loading configuration, the bridge always found alternative paths to transfer the loads.

All these previous studies agreed that twin box–girder steel bridges have significant level of redundancy even with a fully fractured girder. In addition, all the studies noted that in twin box–girder steel bridges alternative paths is always present for the load to transfer in the case of major damage to one of the main girders.

CHAPTER 3

METHODOLOGY AND NUMERICAL MODELING

3.1 The Methodology

Fatigue life of details is generally categorized by two stages; namely crack initiation and crack propagation. These two stages of crack growth are driven by one or a combination of the three different loading modes, which are mode I, mode II, and mode III. These three modes essentially give rise to bending and/or shear stresses, causing the crack to initiate and propagate.

There are two cases where multi-mode loading in steel bridges might arise. The first case is where out-of-plane distortion loading is present in specific details such as transverse connection plates pulling out on a girder web, causing all three modes to participate in crack initiation and growth, with the predominant contribution being from mode III (Mahmoud and Miller 2016). The second case is when the crack length has become sufficiently large, causing large distortion and subsequently giving rise to participation from other modes. This second case is depicted in Fig. 3.1 where eccentricity of the applied load on the deck (Fig. 3.1(a)), in combination with the large crack, cause an out-of-plane twist in the girder (Fig. 3.1(b)).

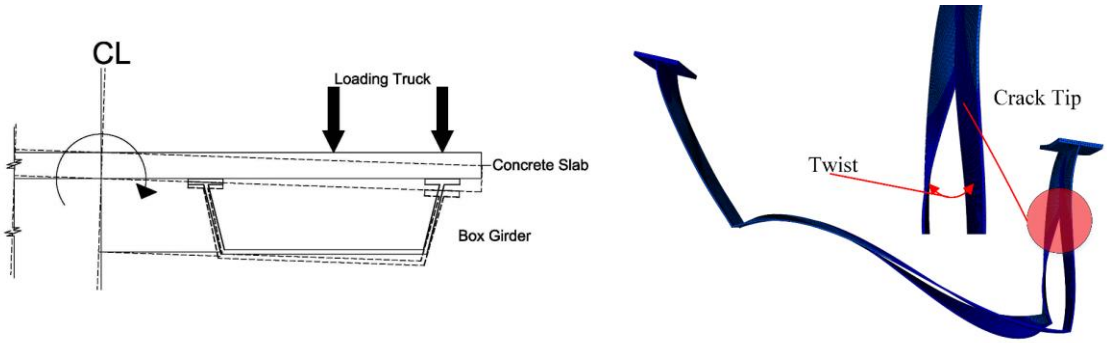

Fig. 3.1. Bridge behavior under applied loads in the presence of a girder crack

When conducting fatigue and fracture assessment, a parameter called the stress intensity factor (SIF) needs to be estimated numerically. The SIF is calculated and 1) compared to a threshold value to determine the onset of crack growth, 2) used to in a crack propagation law to determine the crack growth rate, and 3) compared to a critical value to determine the onset of fracture, marking the end of fatigue life. The determination of the SIF for simple details can realized using closed-form solutions that are available in the literature. However, for complex details, the J-integral can be utilized to compute the energy release (or work per unit fracture surface area) and relate it to the SIF. The J- integral is defined by:

$$J = \int_{\mathbb{\Gamma}} \left(W\, dy - T_i . \frac{\partial u_i}{\partial x}\right) ds \tag{3.1}$$

$$T_i = \sigma_{ij}\, n_j \tag{3.2}$$

Where, W is strain energy density, T is surface tractions, u is the displacement vector, σ_{ij} is the components of the Cauchy stress tensor, n is the normal unit vector, $\mathbb{\Gamma}$ is a curve surrounding the notch tip of the crack, x and y define the coordinate system with x being the direction parallel to the crack plane and y being the direction perpendicular to the crack, and ds is an element of arc on this curve. The releationship between the J- integral and SIF for each mode is defined as:

$$J_I = \frac{K_I^2}{E'} \tag{3.3}$$

$$J_{II} = \frac{K_{II}^2}{E'} \tag{3.4}$$

$$J_{III} = K_{III}^2 \left(\frac{1+\upsilon}{E}\right) \tag{3.5}$$

Where E is the Young's modulus of the material, E' is E for plane stress and $\left(\frac{1-\upsilon^2}{E}\right)$ for plane strain, and υ is Poisson's ratio.

3.1.1 Crack Fatigue Life and Propagation Rate

One of the main objectives for this study is to evaluate the crack growth rate. Various models exist in the literature for assessing fatigue crack growth rate including Paris and Edorgan (1963), Walker (1970), Forman (1972), McEvily (1974), Zheng (1983), Wang et al. (1994), Beden et al. (2009). Paris and Edorgan (1963) hypothesized that the range in SIF factor, ΔK, governs fatigue crack growth. Experimental *da/dN* versus ΔK data typically exhibits a sigmoid growth model when plotted on a log–log scale. There is a ΔK threshold, ΔK_{th}, below which cracks will not propagate. The Paris law is fit to the linear part on a log–log scale above ΔK_{th}. At relatively high ΔK levels, the crack growth rate accelerates, as the fatigue crack growth is accompanied by some ductile tearing or increments of brittle fracture in each cycle. The Paris aw describes the relationship between the crack propagation rate *da/dN* and the SIF range and is defined as follows:

$$\frac{da}{dN} = C\ (\Delta K)^m \tag{3.6}$$

Where, *da* is the crack length increment, *dN* is the number of cycles associated with this crack increment, ΔK is SIF range, which is the difference between the maximum and the minimum SIFs, and *C* and *m* are material constants.

3.1.2 Fracture Assessment and Failure Modes

Assessing the significance of defects in welded connections has been established in various countries through detailed procedures. These procedures are outlined for various industries for variety of critical welded steel structures including pipelines, offshore structures, ships, among others. The most used is the widely accepted British Standard, BS 7910: 2015, *Guide on Methods for Assessing the Acceptability of Flaws in Metallic Structures* (BS 7910 2015), which is based on accepted fracture mechanics principles. Specifically, the Failure Assessment Diagrams (FAD) is

included in BS 7910 to allow for the determination of whether or not a crack or a flaw is acceptable. FAD consists of three elements, which are the fracture axis (y-axis), collapse axis (x-axis), and assessment line. The vertical axis represents K_r, which is indicative of the potential of brittle fracture and represents the ratio of the SIF to the material fracture toughness. The horizontal axis, L_r, is indicative of plastic collapse and represents the ratio of the applied stresses to the yield stress. The assessment line defines the acceptability of the crack through delineating the demarcation of failure as follows:

a) For $L_r \leq L_{rmax}$

$$K_r = (1-0.14\, L_r^2)*\{0.3 + 0.7\, exp(-0.65\, L_r^6)\} \quad (3.7a)$$

b) For $L_r > L_{rmax}$

$$K_r = 0 \quad (3.7b)$$

where, L_{rmax} is the plastic collapse limit and is equal to $(\sigma_y + \sigma_u)/2\sigma_y$

where, σ_y is the yield stress and σ_u is the ultimate stress.

In addition to determining the acceptability of the flaw size, the FAD is also indicative of the failure modes, which can be inferred through dividing the diagram into three zones that begin from the origin and extend linearly to the assessment line. These three distinct regions define brittle fracture when $0 < L_r < 0.62$, elastic-plastic fracture when $0.62 < L_r < 0.95$, and plastic collapse when $0.95\, L_{rmax} < L_r < L_{rmax}$ (Hasanaj et al. 2014). Fig. 3.2 provides an illustration of the FAD and the three distinct failure zones.

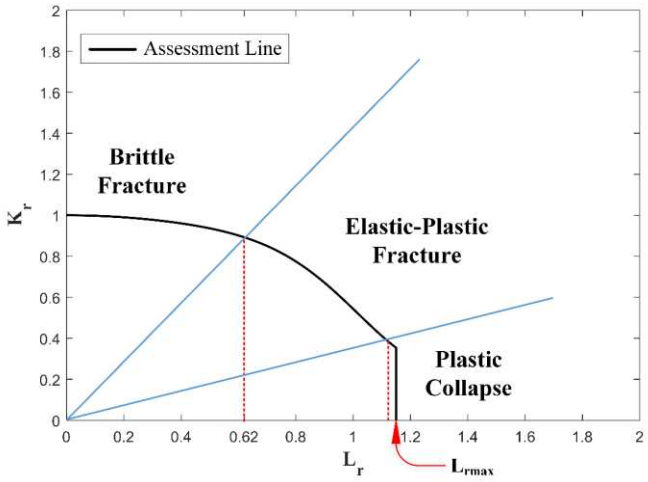

Fig. 3.2. Failure assessment diagram and the failure zones

3.1.3 Through-Thickness Evaluation of SIF

In this study, various SIF values are obtained in the through-thickness direction at each crack increment. However, since only one SIF value is needed for fatigue and fracture assessment at a given crack length, an averaging method is required to obtain only one value. There are various methods available in the literature that can be used to obtain an equivalent SIF value such as the mean values, the root mean square of all through thickness values, and the average values for mid plane. The method utilized in this study is the root mean square, which was shown to produce accurate results in comparison to experimental studies by Seo and Lee (2002) and is defined as follows:

$$K = \sqrt{\frac{K_1^2+K_2^2+K_3^2+\cdots+K_n^2}{n}} \tag{3.8}$$

3.2 Equivalent SIF for Mixed Mode Loadings

Several mathematical models have been proposed to estimate an equivalent SIF that can be used to describe crack propagation under mixed modes of loading (Irwin 1957; Sih 1973; Sih 1975; Burdekin and Yang 1997). Detailed comparison between the different methods for estimating an equivalent SIF under mixed mode was presented by Radaj and Vormwald (2013). The analysis showed that the equivalent SIF estimate proposed by Irwin (1957) results in accurate description of the stress field around the crack tip. Irwin's solution (1957) was based on the resultant energy release rate and ignored the influence of crack propagation angle. The equivalent SIF listed in BS7910 (2015), which is used in this study, yields almost identical results to that of Irwin (1957). It is based on the ratio between material toughness and yield stress, and the ratio between material toughness for different modes. That is if:

$K_{IC} > K_{IIC}$, and

$(K_{mat}/\sigma_y) < 6.3\sqrt{}$mm,

Then the equivalent SIF can be defined as follows:

$$K_{eq} = \sqrt{K_{12}^2 + \frac{K_{III}^2}{(1-\upsilon)}} \tag{3.9}$$

$$\text{Where } K_{12} = \frac{2K_I + 6\sqrt{K_I^2 + 8K_{II}^2}}{8}\left(\frac{K_I^2 + 12K_{II}^2 + K_I\sqrt{K_I^2 + 8K_{II}^2}}{2K_I^2 + 18K_{II}^2}\right)^{\frac{3}{2}} \quad For\ |\frac{K_I}{K_{II}}| \geq 0.466 \tag{3.10}$$

$$\text{And } \quad K_{12} = \frac{|K_{II}|}{0.7} \quad For\ \left|\frac{K_I}{K_{II}}\right| < 0.466 \tag{3.11}$$

3.2.1 Using Mixed Modes SIF for Crack Growth and Fracture Analysis

Following the determination of an equivalent SIFs for mixed-mode loading, the obtained values are utilized in the Paris law crack growth model to assess the propagation rate of the crack.

Development of the Paris law was based on observations of mode I experimental results of crack growth. Therefore, application of the Paris law to predict crack growth rate has largely been restricted to mode I analyses. There are very limited studies in the literature in which crack growth rate under mode II or mode III was correlated to the Paris law. For example, Ritchie et al. (1982) performed experimental testing of 4340 steel samples under torsional loading to evaluate crack growth under mode III. The results of the study showed a correlation between the propagation rates of mode III fatigue loadings to the alternating SIF, ΔK_{III}, in the same fashion as the traditional Paris law. One recent study by Mahmoud and Miller (2016) was conducted in which the use of Paris law for predicting fatigue growth under individual modes and combined modes was assessed. It was shown that fatigue crack growth under multiple modes can be estimated with reasonable accuracy using where an equivalent SIF range, ΔK_{eq}, is used instead of ΔK as:

$$da/dN = C * (\Delta K_{eq})^m \tag{3.12}$$

The premise of using ΔK_{eq} is to transform mixed mode effects into a mode I equivalent. The Paris law constants used for this study are C=9.5E-12 and m=3 (Mahmoud and Riveros 2014), which pertain to mode-I loading. The use of mode I Paris law constants in mixed-mode analysis is reasonable as shown in Xiangqiao et al. (1992).

For the fracture assessment, the issue lies in that both axes of the FAD need to reflect mixed modes of loading. For the brittle fracture axis, (K_r), the equivalent SIF for mode I should be utilized as recommended by BS 7910 (2015). Fracture toughness, (K_{mat}), for mixed mode loading is not available in the literature. Burdekin & Yang (1997) recommended the use of mode-I toughness to represent that of mixed mode. This is particularly acceptable for the case where (K_{mat}/σ_y) is approximately equal to $6.3\sqrt{mm}$ ($1.25\sqrt{in}$), which is the case in this study. If (K_{mat}/σ_y) is larger than $6.3\sqrt{mm}$ ($1.25\sqrt{in}$), then crack extension behavior changes from brittle to ductile with larger

plasticity around the crack tip and the fracture toughness for the mixed mode loading is expected to be much larger than its mode I counterpart (BS 7910 2015). For collapse axis, the reference stress should be calculated to reflect the effect of mixed modes. Under combined multi-axial stresses, the von-Mises stress can be used since it serves as a yielding criterion under multi-directional loading (BS 7910 2015).

3.3 Bridge Topology

To obtain realistic results, an actual bridge is used in the study. The bridge is a steel twin tub girder located on W 44th Avenue, crossing Interstate 25 in Denver, CO. Built in 1988, the bridge is 105.77 m (347 ft) long and 14.33 m (47 ft) wide. Fig. 3.3 shows some pictures of the bridge that used in this study. It is a continuous system, comprising of three spans as shown in Fig. 3.4 (a). Fig. 3.4(b) shows detailed geometry of the girder including the web and flanges thicknesses while Fig. 3.4(c) shows cross section of the bridge geometry illustrating the concrete slab thickness and the steel girders location. One of the objectives of this study is to evaluate the effect of secondary bracings on redistribution of stresses during crack growth and on the potential for fracture. Therefore, two models are developed; one with bracings and one without bracings. The bridge geometry with bracings is shown in Fig. 3.5 (a) while the geometry without bracings is shown in Fig. 3.5(b). Fig. 3.5(c) shows a zoomed-in view of the deck, girders, and bracings.

Fig. 3.3. Images of the bridge that used in this case of study

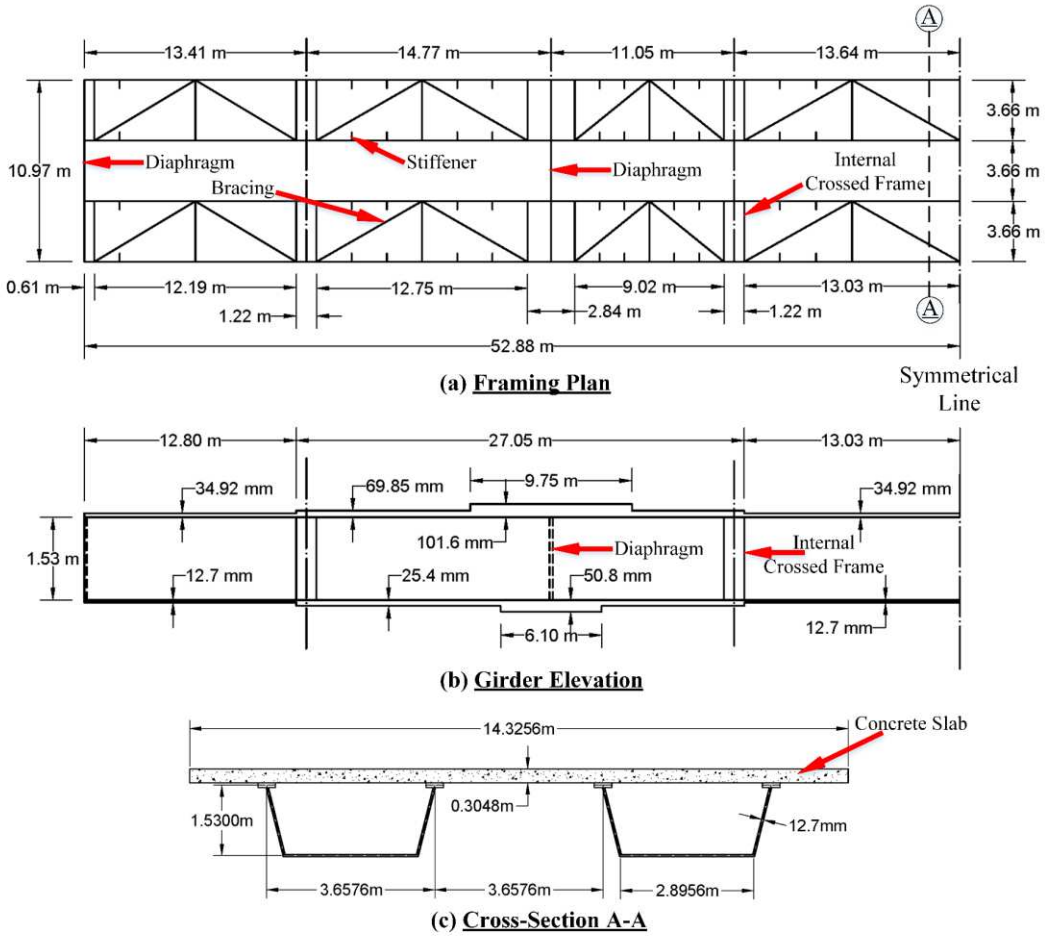

Fig. 3.4. Details of the modeled bridge (a) plan view, (b) girder elevation, and (c) cross sectional view

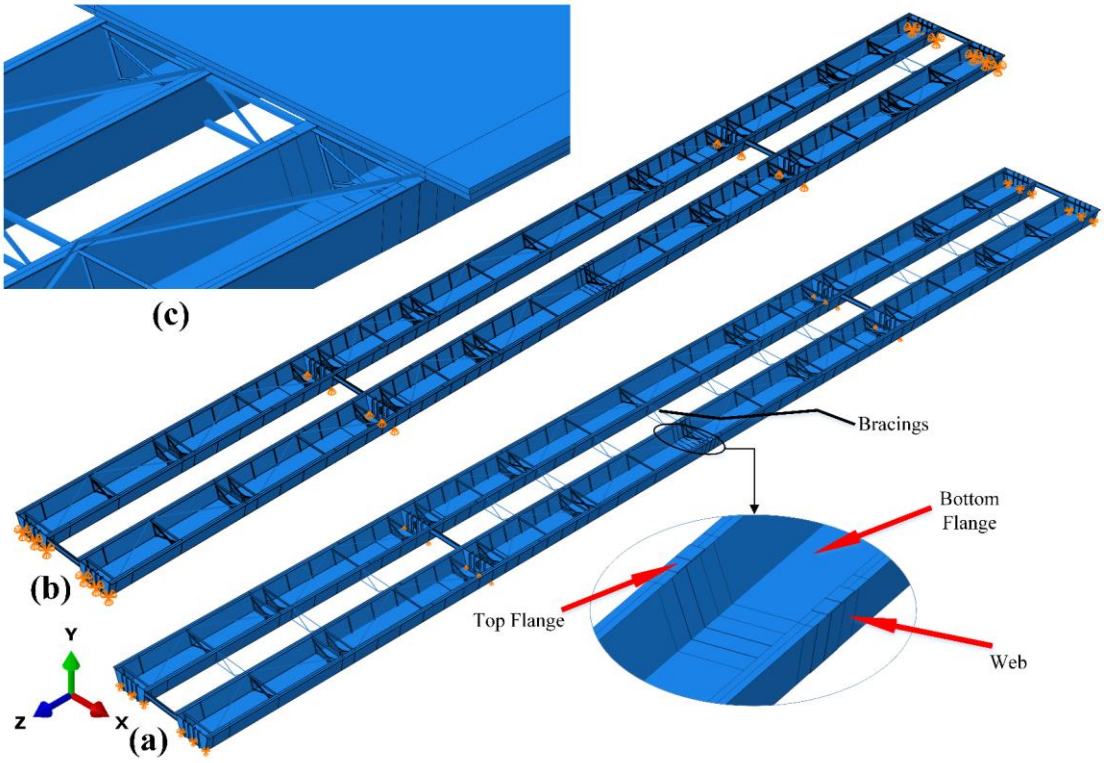

Fig. 3.5. Bridge geometry (a) model with bracings, (b) model without bracings, and (c) zoomed-in view of deck, girders, and bracings

3.4 Numerical Finite Element Modeling

3.4.1 Mesh Definition

Three types of the elements are utilized in the model. These are namely three-nodes quadratic beam in plane (B22) line elements, eight-nodes shell elements with reduced integration (S8R), and twenty-nodes quadratic brick elements with reduced integration (C3D20R) for solid elements. Fig. 3.6 shows and illustrates these three types of element and their integration points. The line elements are used to model the bracings and the shear studs connecting the girders and the concrete slab. The shell elements are used to model the main tub girders, except for the cracked region, and their internal diaphragms as well as the concrete slab. The solid elements are used to model the cracked

region of the girder. The connection between the shell and solid elements is made using shell-to-solid coupling constraint. The use of solid elements allows for the localized stresses around the crack tip to be captured so that accurate estimates of the SIF can be made. Since the value of the SIF is sensitive to the mesh size, mesh refinements are specified around the crack tip. Mesh convergence is also conducted to determine the optimum mesh size. It is determined that a mesh size of 20 mm (0.787 in) or less would be adequate around the crack tip. Therefore, mesh refinement in the cracked region is chosen as 20 mm (0.787 in). Fig. 3.7 (a) shows mesh convergence at 20 mm (0.787 in) and Fig. 3.7(b) shows the detailed mesh for the whole model including the refined region. In this analysis, the crack is modeled by defining the crack length and direction explicitly. The crack length is increased manually at small increment for each run.

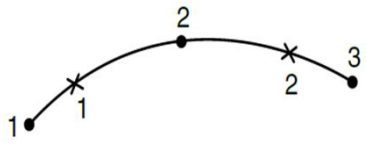

B22: 3-nodes element, 2-integration points

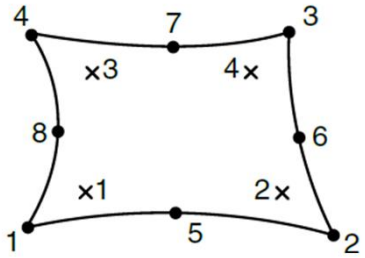

S8R: 8-nodes element, 4-integration points

Hexahedron (brick) element faces

Face 1	1 – 2 – 3 – 4 face
Face 2	5 – 8 – 7 – 6 face
Face 3	1 – 5 – 6 – 2 face
Face 4	2 – 6 – 7 – 3 face
Face 5	3 – 7 – 8 – 4 face
Face 6	4 – 8 – 5 – 1 face

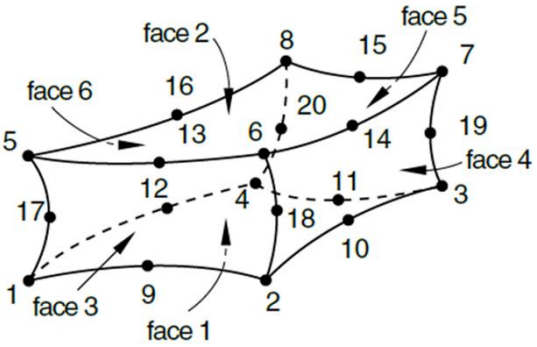

C3D20R: 20-nodes element

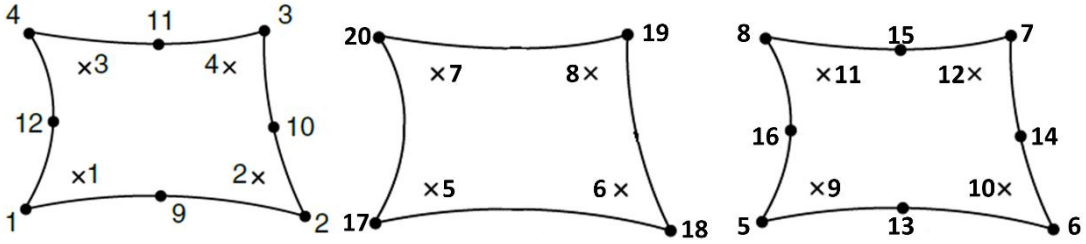

C3D20R: 20-nodes element integration points

- Element node
x Integration point

Fig. 3.6. The elements used in this study types their integration points (*ABAQUS 6.12 Analysis User's Manual, Volume IV: Elements)*

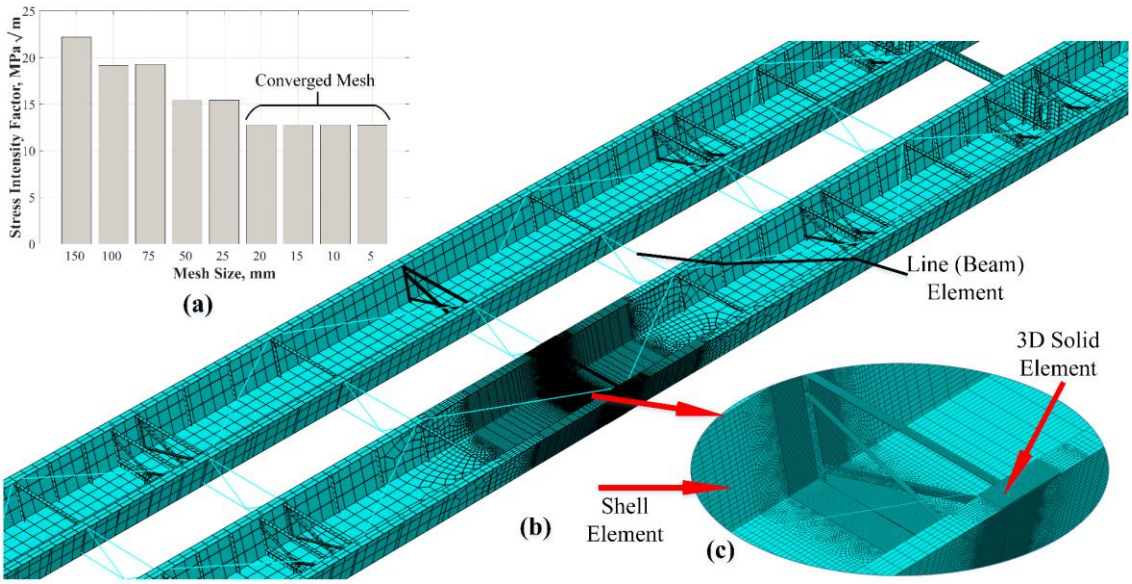

Fig. 3.7. Finite element model and mesh size (a) mesh convergence, (b) entire bridge model, and (c) zoom-in view of the cracked region

3.4.2 Materials Properties

Two types of materials are employed in the numerical finite element model including steel and reinforced concrete. The steel used is grade 50 (A572) with yield stress of 345 MPa (50 ksi), ultimate strength of 448 MPa (65 ksi), elastic modules of 200,000 MPa (29,000 ksi), and Poisson's ratio or 0.3. The reinforced concrete comprises of concrete and reinforcing steel. The concrete used has an elastic modulus of 25,131.39 MPa (3,645 ksi), and a Poisson's ratio of 0.26. The streel rebar is also Grade 50. The reinforced concrete is modeled using two different methods. First, in the elastic analysis, which was conducted to determine the SIF near the crack tip, equivalent values for the steel-concrete composite was utilized based on the approach by (Liu 1997). In addition to the linear analysis, nonlinear simulations are conducted to predict structural collapse under extreme load.

To estimate an equivalent property of the reinforced concrete such as elastic modulus, shear modulus, and Poisson's ratio of the steel rebar – concrete composite, a rule of mixture method is utilized, and it is defined as follows:

$$X_{eq} = \frac{1}{V_{total}} \sum_{1}^{n} V_n * X_n \tag{3.14}$$

Where X_{eq} is the equivalent property, n is the number of combined materials, V_n is the volume of material n, X_n is the property for material n, and V_{total} is the total volume for all materials used. Using the rule of mixture described above, the material properties used in the model for the slab are 25,655.84 MPa (3721 ksi) for the elastic modulus and 0.26 for the Poisson's ratio.

For the nonlinear analysis, the concrete slab is modeled differently where a reinforcing steel rebar net is modeled inside the concrete slab and concrete damage plasticity (CDP) model is defined using the values outlined in Jankowiak and Lodygowski (2005), and Table (3.1) shows the properties for this model.

Table 3.1: The concrete damage plasticity (CDP) model properties Jankowiak and Lodygowski (2005)

Material's parameters	B50	The parameters of CDP model	
		β	38^{o}
Concrete elasticity		m	1
E[GPa]	19.7	$f=f_{b0}/f_c$	1.12
υ	0.19	γ	0.666
Concrete compression hardening		Concrete compression damage	
Stress [MPa]	Crushing strain [-]	Damage C [-]	Crushing strain [-]
15.0	0.0	0.0	0.0
20.197804	0.0000747307	0.0	0.0000747307
30.000609	0.0000988479	0.0	0.0000988479
40.303781	0.000154123	0.0	0.000154123
50.007692	0.000761538	0.0	0.000761538
40.236090	0.002557559	0.195402	0.002557559
20.236090	0.005675431	0.596382	0.005675431
5.257557	0.011733119	0.894865	0.011733119
Concrete tension stiffening		Concrete tension damage	
Stress [MPa]	Cracking strain [-]	Damage T [-]	Cracking strain [-]
1.99893	0.0	0.0	0.0
2.842	0.00003333	0.0	0.00003333
1.86981	0.000160427	0.406411	0.000160427
0.862723	0.000279763	0.69638	0.000279763
0.226254	0.000684593	0.920389	0.000684593
0.056576	0.00108673	0.980093	0.00108673

3.4.3 Crack Definition and Propagation Directions

The crack is assigned at a transverse welded stiffener connection, which is part of an internal cross frame, that is located along the bridge at its mid length. Specifically, the crack is placed in one of the tub girders at the flange-to-web interface as shown in Fig. 3.8. The reason for selecting this region for introducing the crack is because this location represents possible crack initiation site that is subjected to the maximum positive bending moment. The crack is assigned with a starting length of 63.5 mm (2.5 in) and is postulated to include two tips as it propagates in the web and the flange. Fig. 3.8 shows the initial crack location and the directions in which each

crack tip is assumed to have propagated. Since the crack location is such that an unsymmetrical loading is applied to its two tips, the crack growth rate for Tip#1 and Tip#2 will not be the same. The increment of crack growth for each crack is calculated by assuming a typical increment for one of the cracks, calculating the number of cycles for crack growth using the Paris law, then use that number of cycles to determine the increment of crack length for the other crack. The SIFs are then calculated once both cracks have been incremented. For simplification, the increments of crack length are assigned in a straight line along the flange and the web of the girder. The approximation of straight line crack growth is validated by assessing the value of the phase angle expressed as:

$$\Theta = \tan^{-1} (K_{II} / K_I) \quad (3.14)$$

Where K_{II} is the SIF for mode II, and K_I is the SIF for mode I. When $\Theta = 90$ degrees it is pure mode I, and when $\Theta = 0$ degree it is pure mode II. The SIF values for mode I and mode II in this study, obtained from a straight-line crack analysis, are used to determine the resulting crack angle, which is shown to vary mainly between 80-90 degrees (i.e. minimal crack curving). The only two exceptions where crack curving is noted is when the crack length reaches 1,422.4 mm (56 in) for Tip#1 in the web, and 50 mm (2 in) for Tip#2 in the flange, where the crack is still very short. With only two crack length showing potential for crack curving, the assumption of a straight crack is confirmed. Fig. 3.9 demonstrates the phase angle versus the crack length for both tips.

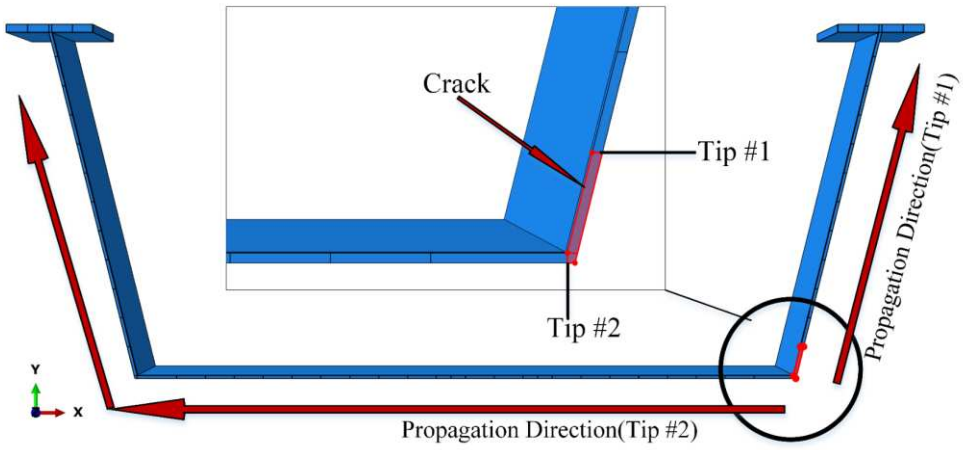

Fig. 3.8. Initial location of the crack and the propagation directions

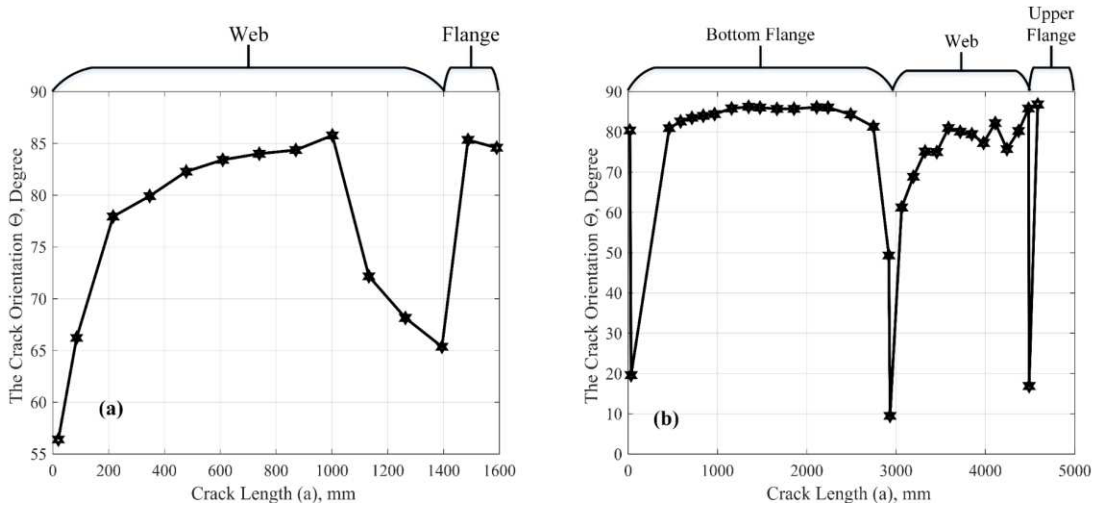

Fig. 3.9. The crack orientation versus the crack length (a) Tip#1 and (b) Tip#2

3.4.4 Applied Loads and Load Cases

The loads assigned to the model are in the form of an HL-93 fatigue truck as per the 2017 AASHTO Specification (2017). This truck has three axles with total force of 320.28 kN (72 kips) that is distributed to two rear axles with 142.34 kN (32 kips), spaced at 9.144 m (30 ft) and steering axle with 35.58 kN (8 kips) spaced with the middle axle at 4.27 m (14 ft). Each axle distributes the force to number of patches. The rear axles distribute their force to four patches that are 508 mm x

254 mm (20 in x 10 in) while the steering axle distributes its force to two patches that are 254 mm x 254 mm (10 in x 10 in). In addition, for fatigue analysis the specification requires the inclusion of 15% dynamic load allowance, for the case where the load is applied statically. In order to obtain the maximum and minimum stress values applied to the detail of interest at the cracked region, two loading cases are considered. For ultimate load analysis, another loading case is defined to produce maximum stresses. The fracture load case includes the first fatigue load case in addition to lane load and dead load (self-weight). The lane load is 0.8677 kN/m (0.64 kips/ft) for a 3.048 m (10 ft) wide lane. This load represents additional traffic load beside the HL-93 truck load. The fracture load case is utilized to assess the fracture modes for several crack lengths and to compare between the calculated SIF and material toughness. In addition to fatigue and fracture loading, another loading case is utilized to assess the potential for system collapse under extreme loading in the presence of full-girder fracture. This case includes dead load (self-weight), live load (loading truck and lane load), and their associated load factor. The load factors are 1.5 and 0.5 for dead load for calculating the von-Mises stresses and the SIFs, respectively, 1.75 for live load, and 1.15 for dynamic allowance. Fig. 3.10 (a) shows boundary conditions for the model, while Fig. 3.10 (b) shows the location of the applied loads with the loads. Fig. 3.10 (c) illustrates the loading application for fatigue analysis. The three loading cases are summarized in Table 3.2.

Table 3.2: Loading cases

Case No.	The Analysis Type	The Included Loads
Case (1)	Fatigue Assessment	HL-93 truck load + 1.15 Dynamic allowance
Case (2)	Fracture Assessment	HL-93 truck load + Lane load + Dead load + 1.15 Dynamic allowance
Case (3)	Collapse Evaluation	1.75 HL-93 truck load + 1.75 Lane load + 1.5 Dead load + 1.15 Dynamic allowance

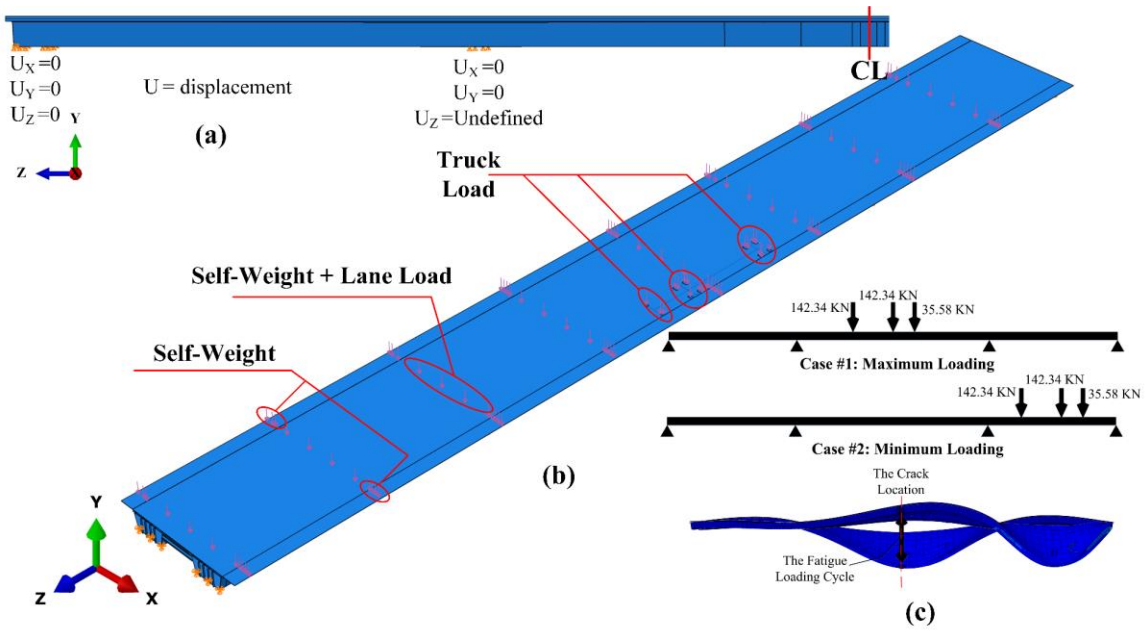

Fig. 3.10. (a) Model boundary conditions, (b) applied loads, and (c) fatigue loading cycle

CHAPTER 4

ANALYSIS RESULTS

4.1 Components of Results

The results presented in this study are for mode I and mixed-mode behavior and include overall deformation of the bridge, total fatigue life of the propagated crack, rate of crack growth, fracture assessment using the FAD, the probability of dynamic crack growth as a function of inspection intervals, and the potential for system collapse.

4.1.1 Global Deformation

The maximum vertical displacement in the Y-direction for the bridge at mid length of the bridge without crack and for case (2) is 56.21 mm (2.213 in) for the model without bracings and 55.22 mm (2.174 in) for model with cross bracings. The maximum vertical displacement increases gradually with increase in crack length until full girder fracture to 83 mm (3.268 in) for the model without bracing and 78 mm (3.071in) for the model with bracings as shown in Fig. 4.1. This corresponds to total increase in displacement by 41%-48% due to full girder fracture. The inclusion of bracings results in 7% reduction in the vertical displacement as well reduction in the stresses concentration around the crack tip, leading to stabilization of the whole bridge, in the presence of full girder fracture, as will be discussed later.

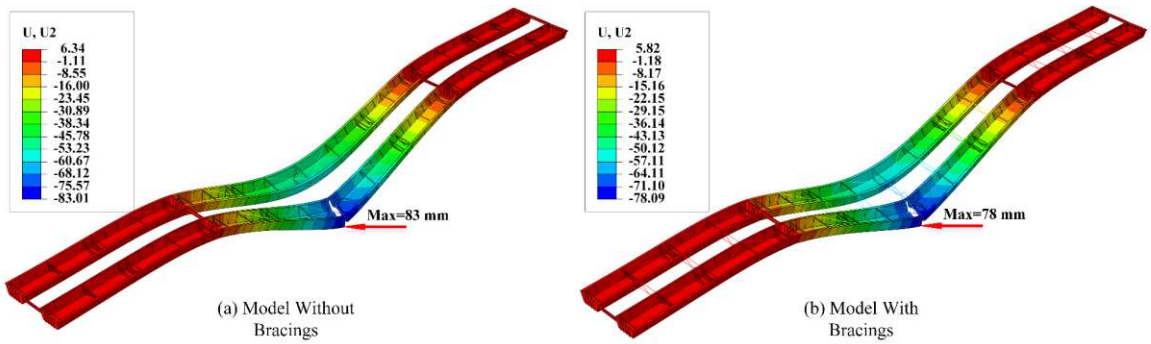

Fig. 4.1. Vertical deformation of the bridge in the presence of a full girder fracture

4.1.2 Crack Fatigue Life

Understanding fatigue crack growth life is critical for devising proper inspection intervals for the bridge. Fig. 4.2 through Fig. 4.6 show the SIF range versus crack length for each of the three modes and the mixed mode for the unbraced and braced models, respectively. The figures show uniform increase in the change in SIF range, ΔK, until the crack reaches the end of the web for Tip#1 and the end of the upper flange for Tip#2. The reason for the drop in the SIF factor due to the upward "shift" in the location of the neutral axis as the crack becomes larger, as mainly evident for mode-I loading. It is also noted that ΔK is similar for mode I and mixed mode for Tip#1 for the entire crack length. For Tip#2, similar observation is noted except after the crack enters the web where noticeable difference between mode I and mixed mode results are seen. In addition, ΔK for Tip#2 shows high scatter through the web. Moreover, a substantial jump in ΔK is observed at the flange web intersection due to the high stress concentration resulting from the abrupt change in geometry. The observed jump in ΔK is followed by substantial reduction once the crack entered the flange.

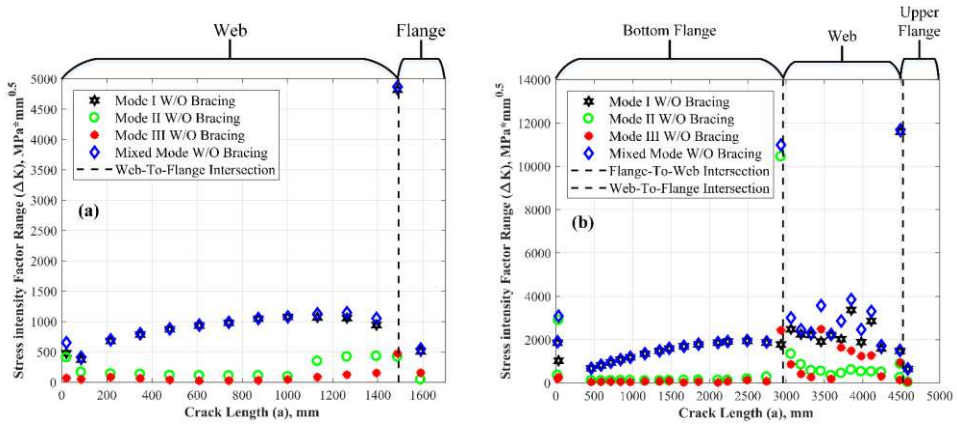

Fig. 4.2. Stress intensity factor range for the model without bracings for all modes (a) Tip#1 and (b) Tip#2

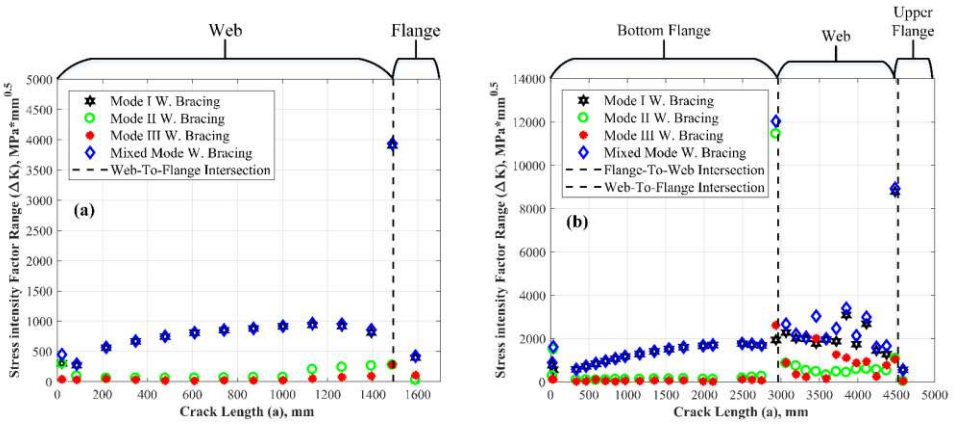

Fig. 4.3. Stress intensity factor range for the model with bracings for all modes (a) Tip#1 and (b) Tip#2

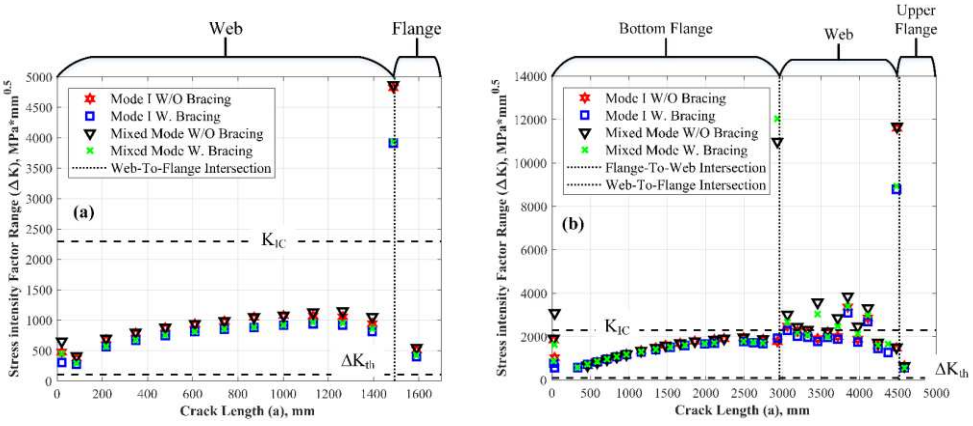

Fig. 4.4. Stress intensity factor range for mode I and mixed mode (a) Tip#1 and (b) Tip#2

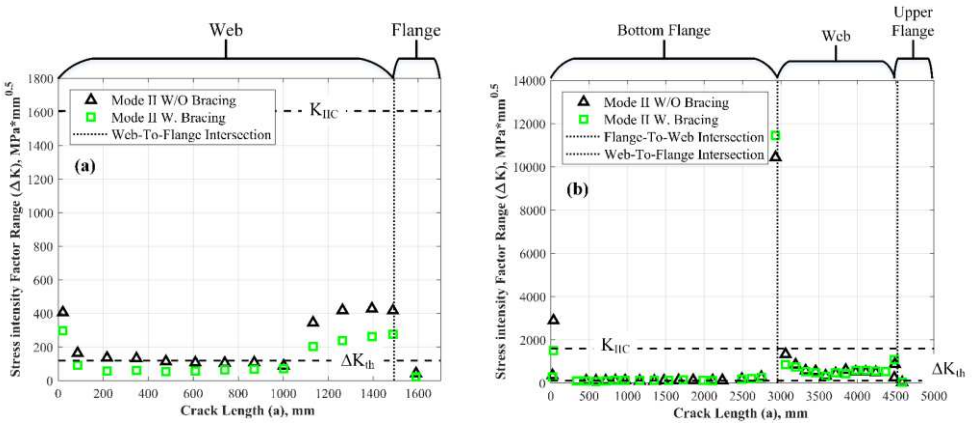

Fig. 4.5. Stress intensity factor range for mode II (a) Tip#1 and (b) Tip#2

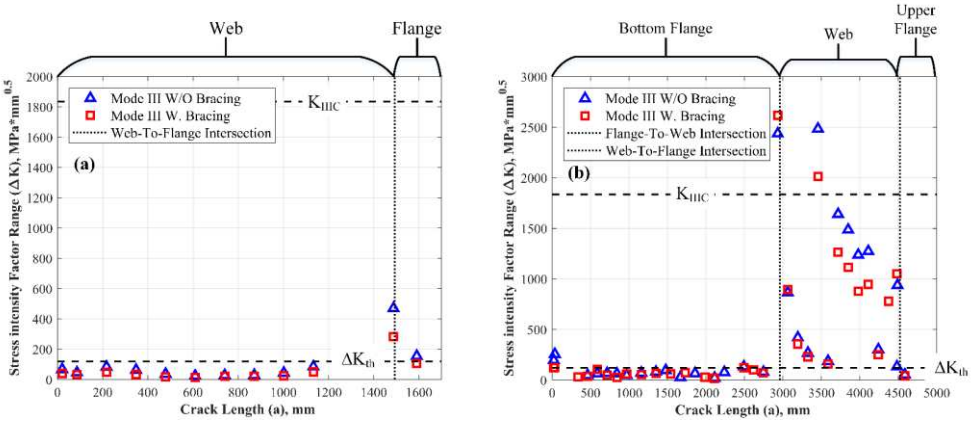

Fig. 4.6. Stress intensity factor range for mode III (a) Tip#1 and (b) Tip#2

Assessment of fatigue crack growth is conducted using the Paris law. A plot of crack length versus number of cycles is shown in Fig. 4.7 (a) for Tip#1 and Fig. 4.7 (b) for Tip#2. The figures show significant difference in the number of cycles for a given crack length between the model with bracings versus the model without bracings. The effect of including only mode I versus the mixed modes is, however, not as significant. Specifically, the inclusion of mode I results in total fatigue life of 1.34E+07 cycles for Tip#1 and 9.85E+06 cycles for Tip#2 for the model without bracings and 2.82E+07 cycles for Tip#1 and 1.29E+07 cycles for Tip#2 for the model with bracings. Including the bracings increases the total number of cycles by approximately 30%-90% on average. The inclusion of the mixed modes results in total number of cycles of 1.09E+07 for

Tip#1 and 9.16E+06 cycles Tip#2 for the model without bracings and 2.35E+07 cycles for Tip#1 and 1.17E+07 cycles for Tip#2 for the model with bracings. The use of mixed mode analysis results in approximately 7%-10% reduction in fatigue life.

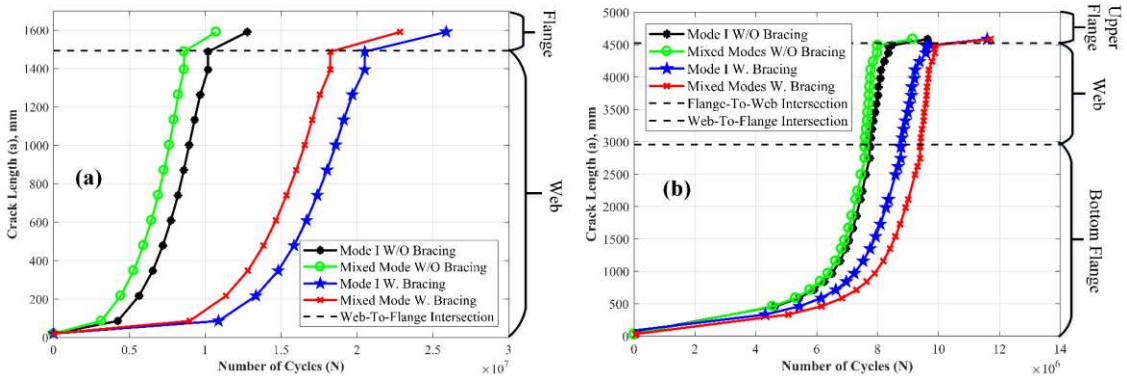

Fig. 4.7. Crack length versus number of cycles (a) Tip#1 and (b) Tip#2

4.1.3 Fracture Assessment

FAD analysis is performed to evaluate the acceptability of the crack and to gain insight on the failure mode and the extent of plastic deformation around the crack tip. In this analysis, case (2) is used for loading. Unlike the fatigue behavior, the fracture appears to be sensitive to the inclusion or exclusion of the various modes. Specifically, the distribution of fracture locus for several crack lengths demonstrates change of the nature of crack propagation and failure mode. In other words, while the crack length is increasing the failure mode changes from brittle to more ductile mode, implying an increase in plastic deformation around the crack tips. Fig. 4.8 demonstrates first mode and mixed mode FAD for both tips and both models. For Tip#1, most of the points land outside the interaction region, indicating unacceptable crack lengths. For Tip#1 under mode I, the majority of these points are dominated by brittle fracture while failure noted by the other points is dominated by transition brittle-ductile failure. The remaining points that landed inside the interaction region are located in the brittle zone indicating brittle fatigue growth. For mixed mode, the location of the

failure points appears to be located in similar zones to that for mode I. Furthermore, the FAD analysis for Tip#1 shows the acceptable crack length to be approximately 190.5 mm (7.5 in) for both models and for both mode I and mixed-mode loadings. It is also observed that including mixed-mode loading forces the crack behavior to be more ductile. For Tip#2, the FAD analysis shows similar observation to Tip#1 except there are some points that are located in the plastic collapse zone, indicating net section failure. This tip undergoes different modes of failure, which starts with brittle behavior then progresses towards a transition mode and end with collapse on the net area. The inclusion of bracings cause reduction in both fracture and stress values while the inclusion of mixed mode results in an increase in these values for both models, especially in the model without bracings, which shows a substantial shift on the collapse axis. Furthermore, the FAD analysis for Tip#2 shows the acceptable crack length to be also 72 mm (2.835 in) for both models and for mode I and mixed-mode loadings. Therefore, the total critical crack length is approximately 262.5 mm (10.34 in).

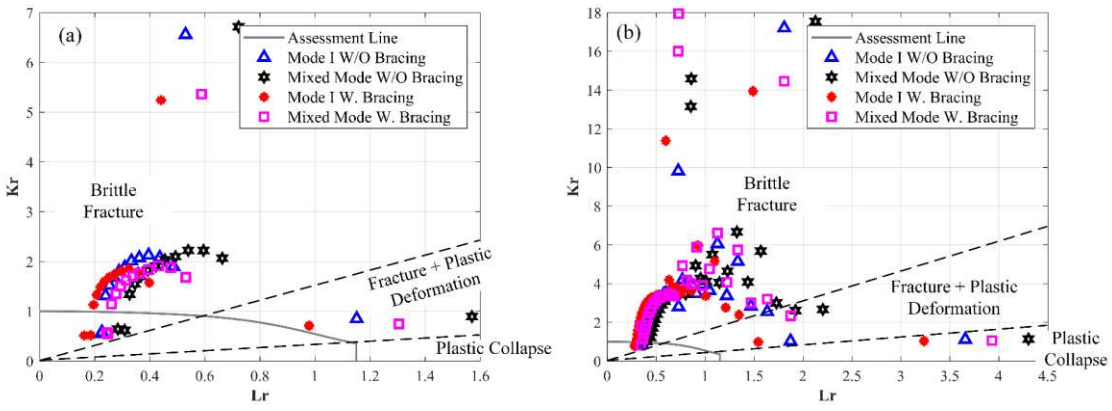

Fig. 4.8. Fracture assessment diagram (a) Tip#1 and (b) Tip#2

4.1.4 Probabilistic Inspection Interval

The SIFs obtained using finite element analysis are used to investigate the effect of statistical variation in the Paris law constants (C & m) on crack propagation where C and m treated as random variables. The variations in the parameters is assumed to follow Normal distribution with mean and standard deviation of 9.5E-12 and 0.25E-12, respectively, for C, and 3 and 0.03, respectively, for m (Mahmoud & Riveros 2014). Fig. 4.9. shows the variation in the number of cycles as function of crack length resulting from the randomness in m and C. The results show the total minimum and maximum number of cycles for Tip#1 to be 5.5042E+06 and 1.8504E+07, respectively. For Tip#2 the total minimum and maximum number of cycles is 6.220E+06 and 1.4757 E+07, respectively.

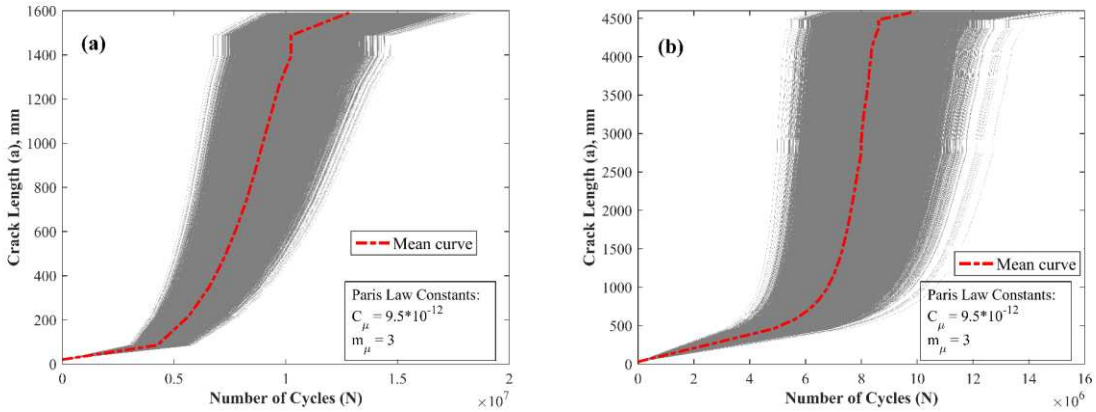

Fig. 4.9. Probabilistic crack length versus number of cycles (a) Tip#1 and (b) Tip#2

The total number of fatigue cycles to failure, however, should be determined at the onset of fracture where unstable crack growth is reached (i.e. $K_{Max} \leq K_{IC}$). Devising proper inspection intervals could, therefore, be based on an acceptable probability of failure by accounting for dynamic fracture. In this study, failure is defined by the inspection interval being smaller than the total number of cycles before reaching a dynamic fracture. This is achieved by setting the fracture toughness, K_{IC}, to be 66.3 $MPa\sqrt{m}$ (60.3 $ksi\sqrt{in}$) (Wright, 2002), which corresponds to 34 Joules

(25 ft-lb) Charpy value in the AASHTO *Specification*. Fig. 4.10 (a) and (b) represent the probability of failure versus inspection interval for crack Tip#1 and Tip#2, respectively. It should be noted that the calculated number of cycles can be translated into intervals in terms of years based on the average daily truck traffic for the bridge. The results show that for a given inspection interval, the highest probability of failure is observed for Tip#1 for Tip#2 under mixed mode without bracings. In general, the most conservative results, yielding the lowest probability of failure, is for the case of mode I with bracings for Tip#1 and Tip#2. It is assumed that once inspection is made and repair is performed, the fatigue life is reset to zero. The new inspection interval should be similar to what have already been calculated.

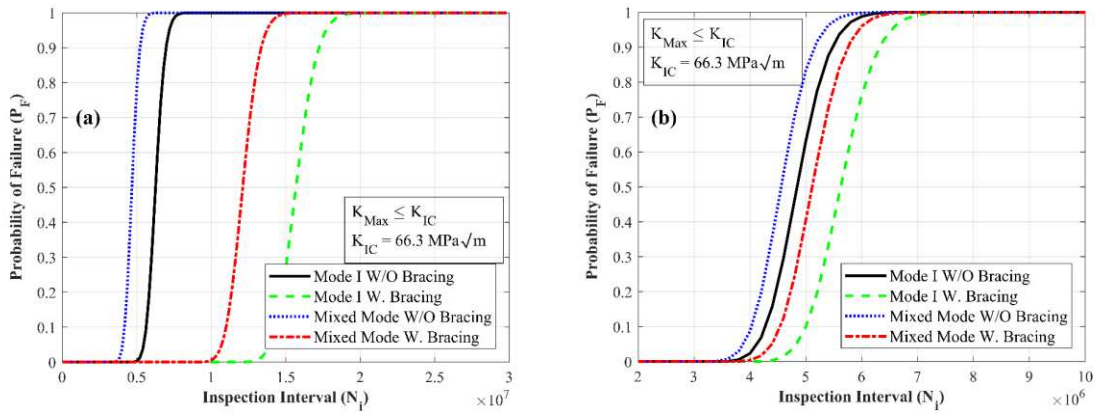

Fig. 4.10. Probability of failure versus inspection interval when $SIF_{Max} \leq K_{IC}$ and for C_μ = 9.5E-12 and m_μ = 3 (a) Tip#1 and (b) Tip#2

To investigate the effect of different statistical variation of C and m on the probability of failure and the corresponding inspection interval, a Normal distribution with mean and standard deviation of 5.21E-13 and 1.2E-13, respectively, for *C* and a value of 3 for *m* are used as per BS 7910 (2005). Fig. 4.11 shows the probability of failure versus inspection intervals for the parameters used. Similar to the previous observations, the results show the highest probability of failure for Tip#1 and Tip#2 to be under mixed mode without bracings.

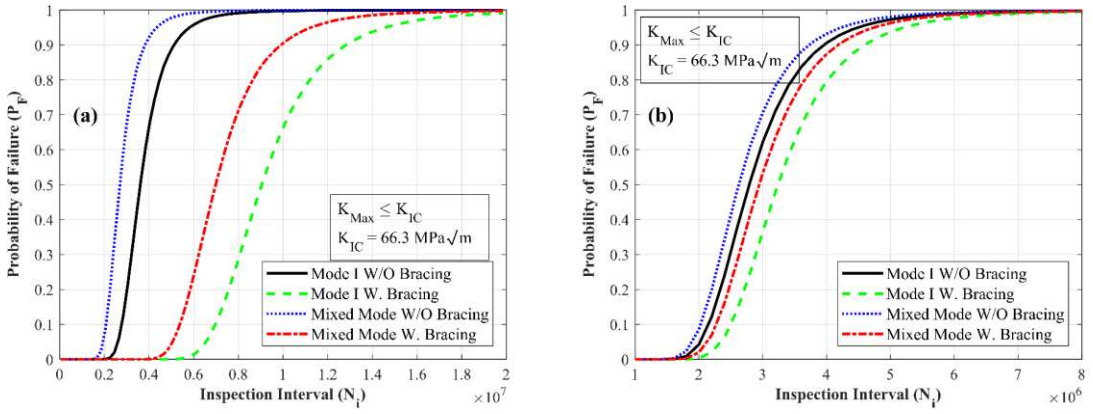

Fig. 4.11. Probability of failure versus inspection interval for $SIF_{Max} \leq K_{IC}$ and for C_μ = 5.21E-13 and m = 3 (a) Tip#1 and (b) Tip#2

To take a closer look into the effect of different statistical variation of C and m on the probability of failure and the corresponding inspection interval, a comparison of the results is made using only the mixed mode without bracings analysis since it represents the worst case scenario. In this comparison both previous statistical variation of C and m of Mahmoud & Riveros (2014) study and BS7910 (2005) are used. Fig. 4.12. (a) and (b) illustrate probabilities of failure for different statistical variation of C and m for both crack tips where Fig 4.13. (a) and (b) represent the reliability index that corresponds to these probabilities of failure. This comparison shows that the results of using different statistical values of C and m result in approximately 40% - 50% difference in the total number of cycles. The large difference in the results when using these statistical data highlight the importance of using probabilistic analysis to estimate reasonable inspection intervals.

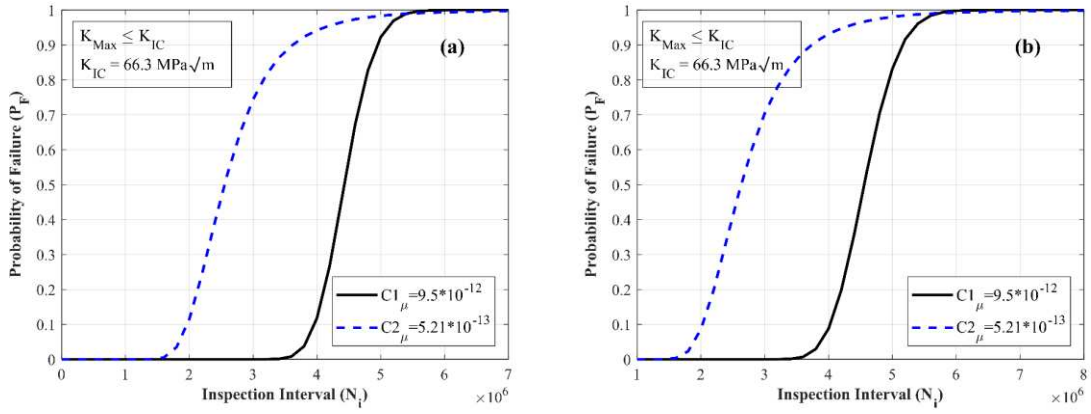

Fig. 4.12. Comparison for different statistical variation of C and m on the probability of failure and the corresponding inspection interval (a) Tip#1 and (b) Tip#2

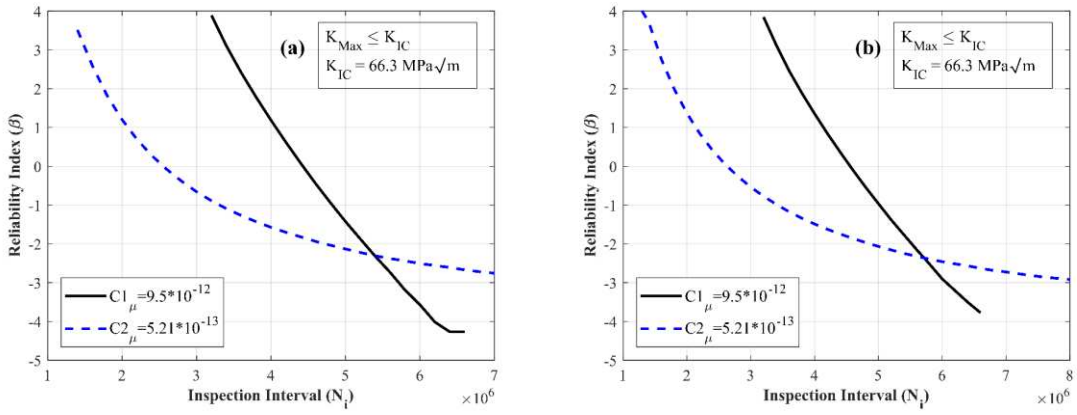

Fig. 4.13. Reliability index vs. inspection interval for different statistical variation of Paris law constants (a) Tip#1 and (b) Tip#2

In the previous analysis, determination of the probability of failure is based on a total number of cycle that corresponds to a deterministic material toughness value. In this analysis, randomness in the fracture toughness is also considered. The coefficient of variation in material toughness ranges between 0.1 - 0.3 as noted in BS 7910 (2015). The mean value used in the analysis is 66.3 $MPa\sqrt{m}$ (60.3 $ksi\sqrt{in}$), which corresponds to what is in the AASHTO *Specification* (Wright, 2002), and the coefficient of variation is 0.3. Fig.4.14. shows several probabilities of failure and their mean

for both crack tips. The reason for the mean curve to show a probability of failure above zero (~1%) with smaller inspection interval is due to the presence of very small fracture toughness values as low as 15 $MPa\sqrt{m}$ (13.65 $ksi\sqrt{in}$) . These small values made the fatigue life very small. This highlights the importance of statistical analysis and its potential use for devising inspection intervals. Fig. 18 shows the reliability index that corresponds to the mean probabilities of failure for both crack tips, with a maximum reliability of 2.7 as shown in Fig. 4.15.

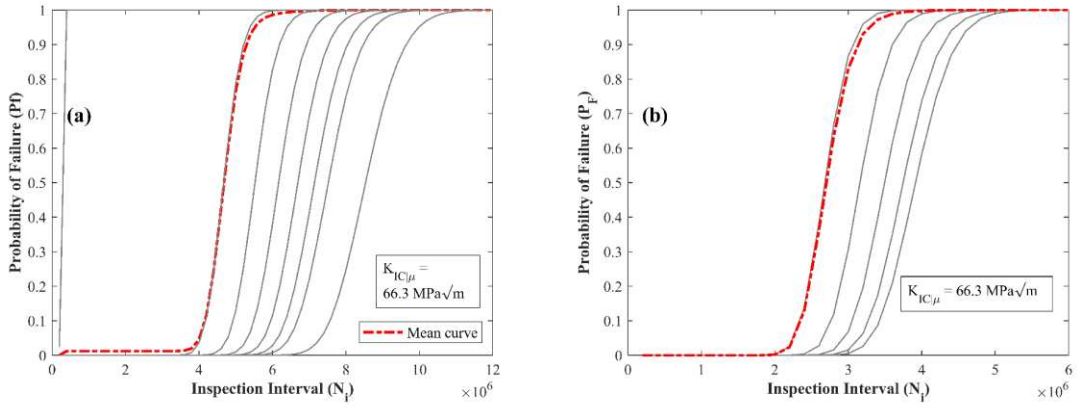

Fig. 4.14. Probability of failure versus inspection interval for variation in the fracture toughness (K_{IC}) (a) Tip#1 and (b) Tip#2

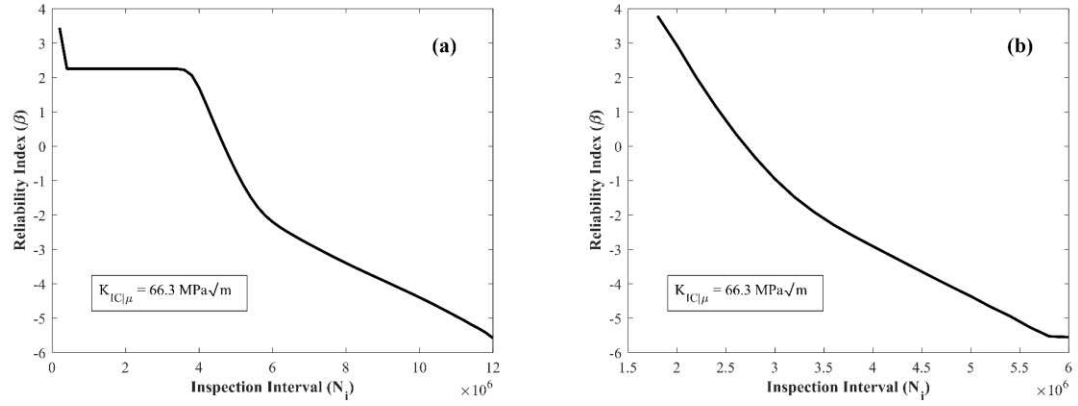

Fig. 4.15. Reliability index versus inspection interval for variation in the fracture toughness (K_{IC}) for (a) Tip#1 and (b) Tip#2

4.1.5 Collapse Evaluation

In concluding this study, analysis is conducted to evaluate the potential for bridge collapse as a result of full girder fracture. For this purpose, plastic analysis is performed to estimate the equivalent plastic strain in the various bridge elements and compare the resulting value to the failure strain for steel and concrete, which are 0.2 and 0.002, respectively. This analysis is conducted with case (3) loadings, which represents an extreme loading scenario. The results show that the model with bracings has higher equivalent plastic strain values than the model without bracings. Although the bracings are shown to help redistribute the stresses and increase fatigue life, they increase the potential for fracture due to the high strain concentration at their connection. These high values are present when the crack reaches a length of approximately 3,440 mm (135.4 in). The results for the model without bracings show the maximum plastic strain to be concentrated around the crack tips and it is the highest when the crack reaches 4,555 mm (179.4 in) in length. Other locations that show large deformations are inner cross frames and around the crack tips. Another interesting result that is noticed in this plastic analysis for both models is that when the crack reaches the top flanges the plastic strain is concentrated in the flange-to-web interface. However, when the crack starts to propagate through the top flanges, the plastic zone becomes very small and negligible. For the concrete slab, both models show yielding in the slab under tension when the girder is fully separated; however, the failure strain is not reached. Fig.4.16. (a) shows the equivalent plastic strain distribution for the concrete slab while Fig.4.16 (b) shows the von-Mises stress distribution for the concrete slab. Fig.4.16 (c) shows the equivalent plastic strain distribution for the steel members while Fig. 4.16 (d) shows von-Mises stress distribution for the steel members. Fig. 4.17 (a) and (b) illustrate the plastic strain location in both models. The maximum von-Mises stress is 14.49 MPa (2.10 ksi) for the concrete slab and 692.26 MPa (100.4

ksi) for the steel members while the maximum equivalent plastic strain is 1.60E-05 for the concrete slab and 1.92E-02 for the steel members. These equivalent plastic strain values are lower than that of the fracture strain. Therefore, the bridge is not at risk of collapse, unless other limit state controls. The bridge in both models shows the maximum displacement to be approximately 90.95 mm (3.581 in) in the vertical direction. In conclusion, the bridge in both models is not at risk of collapse after one of its girders is fully fractures.

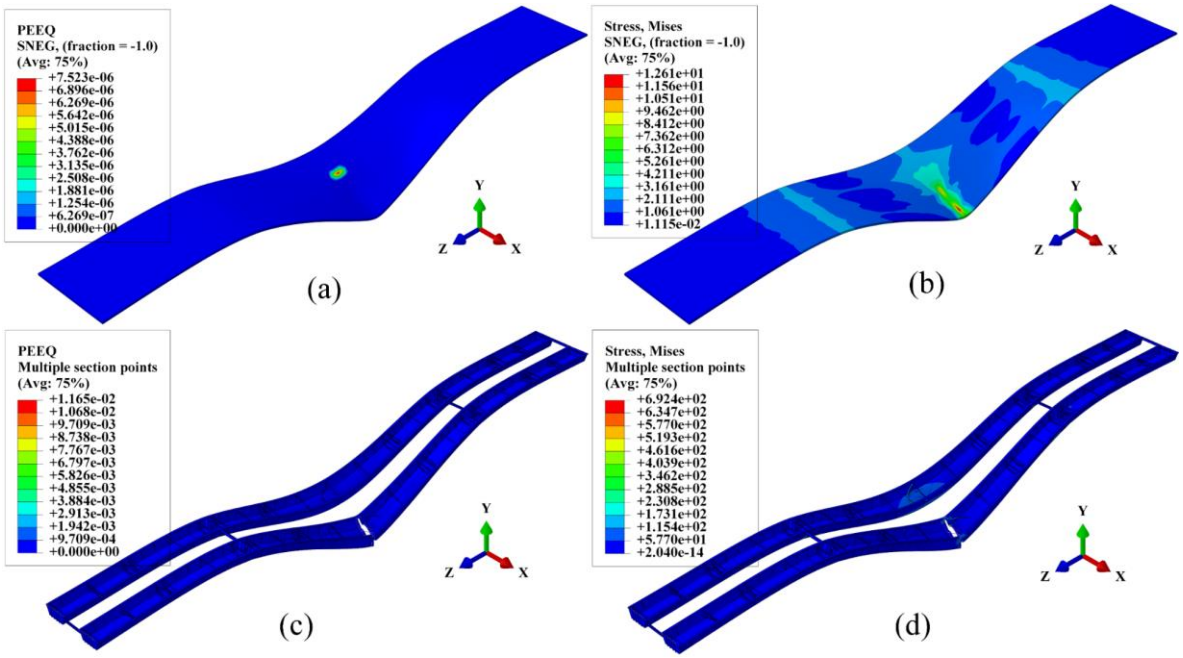

Fig. 4.16. (a) Equivalent plastic strain distribution for the concrete slab, (b) Von-Mises stress distribution for the concrete slab, (c) equivalent plastic strain distribution for the steel members, and (d) von-Mises stress distribution for the steel members

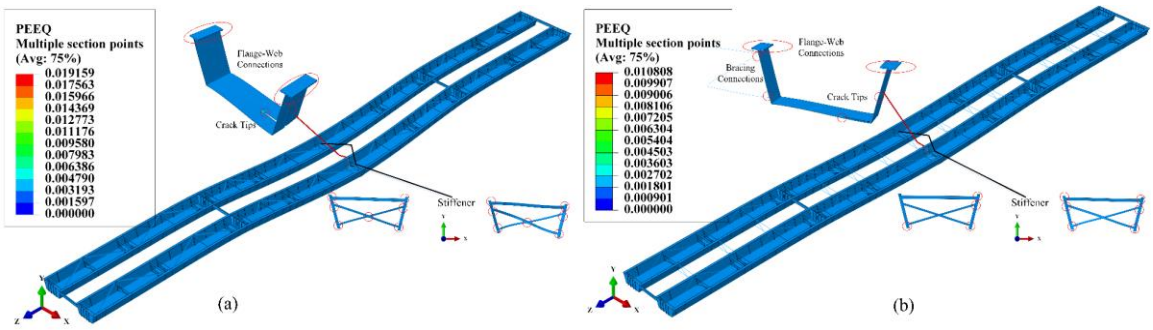

Fig. 4.17. The plastic strain locations (a) the model without bracings (b) the model with bracings

CHAPTER 5

SUMMARY, CONCLUSIONS, AND FUTURE WORK

In this study, finite elements simulations were conducted to evaluate fatigue crack propagation life and failure mode for a steel two box-girders bridge. The analysis utilized the SIF values for a given crack length to 1) draw comparison between the SIF for the three modes of loading as well as mixed mode and to 2) point out the critical crack length for second and third modes of loading. The SIF values were also used to illustrate the effect of cross frames on fatigue crack propagation rate and failure mode. In addition, the results were used in a statistical analysis to determine the probability of failure in terms of inspection intervals. Finally, the study was concluded by evaluating the potential for collapse in case of full girder fracture.

It is important to highlight the value in the probabilistic crack growth analysis conducted in this study for devising inspection intervals. This importance stems from the fact that current inspection scheduling and techniques are based on crack initiation without taking advantage of the considerable fatigue life that can be offered during the propagation stage. In addition, while civil structures in general, and specifically bridges, have demonstrated the ability to tolerate long cracks, assessing the sizes of these cracks deterministically might not be practical. This is because the inherent complexity and scatter associated with fatigue phenomenon mandates that a probabilistic approach be used for the assessment of fatigue life of the details in question. Furthermore, the results of these probabilistic analysis can be further used in life-cycle analysis to determine or even minimize the expected life-cycle cost, resulting in substantial savings in costs associated with inspection and management of bridges. Overall, the study provides useful insight on probabilistic

crack growth and the potential fatigue life extension that can be achieved. The following conclusions can be drawn from the study:

- The crack propagated in a stable manner under first and mixed modes until the fracture toughness specified in the analysis is reached.
- The crack was arrested when interacted with the upper flange.
- High SIF values were present for the second and third modes at the intersection between the webs and the flanges.
- Including mixed mode resulted in reduction in fatigue life by ~ 7% - 10%.
- The inclusion of cross frames as bracings increased fatigue life by ~30% - 90%.
- The FAD analysis showed that an increased crack size changes the crack behavior from brittle to ductile.
- The statistical analysis of crack growth highlighted the scatter in estimating the critical crack size and the corresponding number of cycles.
- The probability of failure versus inspection interval analysis showed the dominant failure case to be the mixed mode for the model without bracings.
- The plastic analysis showed areas of concentrated yielding with no risk of collapse since the equivalent plastic strain did not reach the failure strain for the steel or the concrete.

The research of this thesis raised the need for future work regarding fatigue crack life in two-girder steel bridges, some of this future work include:

- Investigating the effect of mixed mode fracture on other steel bridge configurations such two-girder steel bridges.
- Studying the effect of multiple cracks on fatigue crack propagation life and fracture.

- Evaluating the effects of other transverse elements such as floorbeams or horizontal cross bracings girders on system redundancy and potential collapse.

REFERENCES

AASHTO. 2017. *AASHTO LRFD Bridge Design Specifications*. 8th ed. Washington. DC: AASHTO.

Anderson, T. L. 2005. *Fracture mechanics: fundamentals and applications*. Boca Raton, FL: CRC press.

Barnard, T., Hovell, C. G., Sutton, J. P., Mouras, J. M., Neuman, B. J., Samaras, V. A., ... & Frank, K. H. (2010). *Modeling the response of fracture critical steel box-girder bridges* (No. FHWA/TX-10/9-5498-1). University of Texas at Austin. Center for Transportation Research.

Beden, S. M., Abdullah, S., & Ariffin, A. K. 2009. "Review of fatigue crack propagation models for metallic components." *European Journal of Scientific Research*, 28 (3): 364-397.

British Standards Institution. 2005. *Guide on methods for assessing the acceptability of flaws in metallic structures*. British Standards Institution, London, UK.

British Standards Institution. 2015. *Guide on methods for assessing the acceptability of flaws in metallic structures*. British Standards Institution, London, UK.

Burdekin, F. M., & Yang, G. J. 1997. *Failure assessment diagrams for mixed mode loading and cracked tubular joints*. Advances in Fracture Research, Proceedings of the Ninth International Conference on Fracture, Sydney, Australia, 1: 27-3.

Cha, H., Lyrenmann, L., Connor, R. J., & Varma, A. H. 2014. Experimental and numerical evaluation of the postfracture redundancy of a simple span truss bridge. *Journal of Bridge Engineering*, 19(11).

Connor, R. J., Dexter, R. J., & Mahmoud, H. 2005. *Inspection and management of bridges with fracture-critical details: a synthesis of highway practice* (Vol. 354). Transportation Research Board of The National Academies, Washington, D.C.

Cross, B. T. 2007. *Analysis of the AASHTO fatigue design provisions for welded steel bridge details using reliability theory*. University of Delaware.

Daniels, J. H. 1989. *After-fracture redundancy in steel two-girder bridges*. NCHRP Report 319, Transportation Research Board of The National Academies, Washington, D.C.

Dowling, N. E. 2013. Mechanical behavior of materials: materials, engineering methods for deformation, fracture, and fatigue. 4th ed. UK. Pearson.

Duan, J., Jiang, T., Wei, J., & Long, W. 2015. Relation between strain energy release rates and generalized stress intensity factors for V-shaped notches. In *Measuring Technology and Mechatronics Automation (ICMTMA), 2015 Seventh International Conference on* (pp. 802-806). IEEE.

Forman, R. G. 1972. "Study of fatigue crack initiation from flaws using fracture mechanics theory." *Engineering Fracture Mechanics*. 4 (2): 333–345.

Frank, K. H. 1993. "Notch toughness variability in bridge steel plates." *Journal of the Transportation Research Board*. Vol. 355.

Hasanaj, A., Gjeta, A., & Kullolli, M. 2014. "Analyzing defects with failure assessment diagrams of gas pipelines." *International Journal of Mechanical, Aerospace, Industrial, Mechatronic and Manufacturing Engineering*, 8 (5): 1032-1034.

Idriss, R. L., White, K. R., Woodward, C. B., & Jauregui, D. V. 1995. "Evaluation and testing of a fracture critical bridge." *NDT & E International.* 28 (6): 339-347.

Irwin, G. R. (1956). "Onset of fast crack propagation in high strength steel and aluminum alloys." *NAVAL RESEARCH LAB WASHINGTON DC*. (No. NRL-4763)

Irwin, G. R. 1957. "Analysis of stresses and strains near the end of a crack traversing a plate." *Journal of applied mechanics. 24* (3): 361-364.

Irwin, G. R. (1961). "Plastic zone near a crack and fracture toughness." *Sagamore Research Conference Proceedings,* Vol. 4, 1961 Syracuse University Research Institute, Syracuse NY pp. 63–78.

Inglis, C. E. (1913). “Stresses in a plate due to the presence of cracks and sharp corners.” *Trans Inst Naval Archit*, *55*, 219-241.

Jankowiak, T., & Lodygowski, T. 2005. “Identification of parameters of concrete damage plasticity constitutive model.” *Foundations of civil and environmental engineering*. 6 (1): 53-69.

Liu, G. R. 1997. “A step-by-step method of rule-of-mixture of fiber-and particle-reinforced composite materials.” *Composite structures*, 40 (3-4): 313-322.

Mahmoud, H., & Riveros, G. A. 2013. *Fatigue repair of steel hydraulic structures (SHS) using carbon fiber reinforced polymers (CFRP): feasibility study*. U.S. Army Engineer Research and Development Center, Information Technology Laboratory, Vicksburg, MI.

Mahmoud, H., & Riveros, G. 2014. “Fatigue reliability of a single stiffened ship hull panel.” *Engineering Structures.* 66: 89-99.

Mahmoud, H. N., & Miller, P. A. 2016. “Distortion-induced fatigue crack growth. *Journal of Bridge Engineering*. 21 (2).

McEvily, A. J., 1974. *Phenomenological and microstructural aspects of fatigue*. Presented at the Third International Conference on the Strength of Metals and Alloys, Cambridge, England; published by The Institute and The Iron and Steel Institutes, Publication, W36, 204-213.

Neuman, B. J. (2009). *Evaluating the redundancy of steel bridges: Full-scale destructive testing of a fracture critical twin box-girder steel bridge* (Doctoral dissertation, University of Texas at Austin).

NTSB. 1971. *Collapse of U.S. 35 Bridge, Point Pleasant, West Virginia, December 15, 1967*. Report NTSB-HAR-71-1, National Transportation Safety Board, Washington, D.C.

Paris, PC., and Erdogan, F. 1963. “A critical analysis of crack propagation laws”. *Journal of Basic Engineering; Transaction, American Society of Mechanical Engineers,* Series D, 85: 528-534.

Pham, H., Gull, J. H., Mohammadi, A., & Azizinamini, A. (2016). Managing Florida's fracture critical bridges-phases 1 and 2.

Radaj, D., & Vormwald, M. 2013. *Advanced methods of fatigue assessment*. Heidelberg, Germany: Springer.

Ritchie, R.O., and et.al. 1982. "Mode III fatigue crack propagation in low alloy steel." *American Society of Metals and the Metallurgical Society of AIME.* 13 (1): 101-109.

Seo, D-C. and Lee, J-J. 2002. "Fatigue crack growth behavior of cracked aluminum plate repaired with composite patch." *Composite Structures*, 57: 323–330.

Sih, G. C. 1973. *Handbook of stress-intensity factors*. Lehigh University, Institute of Fracture and Solid Mechanics.

Sih, G. C. (1974). Strain-energy-density factor applied to mixed mode crack problems. *International Journal of fracture*, *10*(3), 305-321.
Sih G. C. 1975. A three-dimensional strain energy density factor theory of crack propagation. In: Three-dimensional crack problems. Leyden, Noordhoff, 15–80.

Walker, EK., 1970. "The effect of stress ratio during crack propagation and fatigue for 2024-T3 and 7076-T6 aluminum. In: Effect of environment and complex load history on fatigue life." *ASTM STP 462*. Philadelphia: American Society for Testing and Materials, pp.1–14.

Wang, W. and Thomas, C. 1994. "Fatigue Crack Growth Rate of Metal by Plastic Energy Damage Accumulation Theory." *Journal of Engineering Mechanics*, 120 (4): 776-795.

Wright, W. J. 2002. Fracture toughness requirements for highway bridges: past and future trends. *Progress in Structural Engineering and Materials*, 4 (1): 96-104.

Xiangqiao, Y., Shanyi, D., & Zehua, Z. 1992. mixed-mode fatigue crack growth prediction in biaxially stretched sheets. *Engineering fracture mechanics*, 43 (3): 471-475.

Yakel, A. J., Azizinamini, A., Pham, H., & Doust D, S. 2014. Comprehensive Evaluation of Fracture Critical Bridges. Nebraska Department of Transportation Research Reports, NDOR Research Project Number SPR-P1(09) P321.

Zheng, Xiulin and A. Manfred, 1983. “Fatigue Crack Propagation in Steels”. *Engineering Fracture Mechanics*, 18(3): 965-973.

Zimmermann, E. A., Launey, M. E., & Ritchie, R. O. 2010. “The significance of crack-resistance curves to the mixed-mode fracture toughness of human cortical bone.” *Biomaterials*, 31 (20): 5297-5305.